Cell Reports

Resource

Human Huntington's Disease iPSC-Derived Cortical Neurons Display Altered Transcriptomics, Morphology, and Maturation

Graphical Abstract

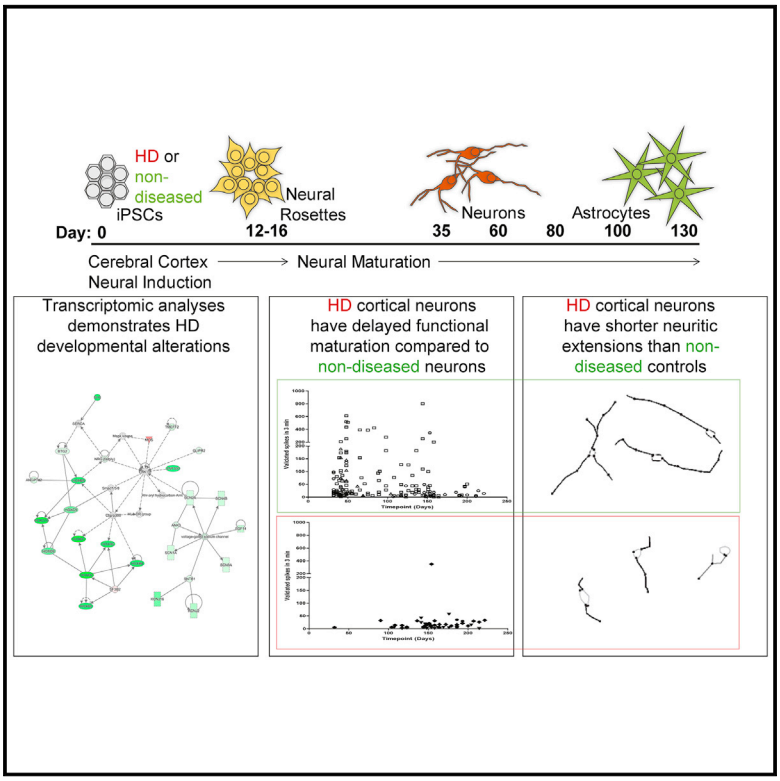

Authors

Shagun R. Mehta, Colton M. Tom, Yizhou Wang, ..., Pranav P. Mathkar, Jie Tang, Virginia B. Mattis

Correspondence

virginiamattis@gmail.com

In Brief

Mehta et al. show that induced pluripotent stem cells (iPSCs) from Huntington's disease (HD) patients can successfully differentiate into functional cerebral cortical neurons. However, the resulting HD cortical neurons display altered transcriptomics and morphological and functional phenotypes indicative of altered corticogenesis in HD.

Highlights

- Differentiated HD and non-diseased iPSCs into functional cortical neurons
- HD iPSC-derived cortical neurons display altered transcriptomics
- HD iPSC-derived cortical neurons display altered morphology
- HD iPSC-derived cortical neurons display altered functional phenotypes

Mehta et al., 2018, Cell Reports *25*, 1081–1096
October 23, 2018
https://doi.org/10.1016/j.celrep.2018.09.076

CellPress

Cell Reports
Resource

Human Huntington's Disease iPSC-Derived Cortical Neurons Display Altered Transcriptomics, Morphology, and Maturation

Shagun R. Mehta,[1,2,5] Colton M. Tom,[1,2,5] Yizhou Wang,[3] Catherine Bresee,[4] David Rushton,[1,2] Pranav P. Mathkar,[1,2] Jie Tang,[3] and Virginia B. Mattis[1,2,6,*]

[1]The Board of Governor's Regenerative Medicine Institute, Cedars-Sinai Medical Center, Los Angeles, CA 90048, USA
[2]Biomedical Sciences, Cedars-Sinai Medical Center, Los Angeles, CA 90048, USA
[3]Genomics Core Facility, Cedars-Sinai Medical Center, Los Angeles, CA 90048, USA
[4]Biostatistics & Bioinformatics Research Center, Samuel Oschin Comprehensive Cancer Institute, Cedars-Sinai Medical Center, Los Angeles, CA 90048, USA
[5]These authors contributed equally
[6]Lead Contact
*Correspondence: virginiamattis@gmail.com
https://doi.org/10.1016/j.celrep.2018.09.076

SUMMARY

Huntington's disease (HD) is a neurodegenerative disease caused by an expanded CAG repeat in the Huntingtin (*HTT*) gene. Induced pluripotent stem cell (iPSC) models of HD provide an opportunity to study the mechanisms underlying disease pathology in disease-relevant patient tissues. Murine studies have demonstrated that HTT is intricately involved in corticogenesis. However, the effect of mutant Hungtintin (mtHTT) in human corticogenesis has not yet been thoroughly explored. This examination is critical, due to inherent differences in cortical development and timing between humans and mice. We therefore differentiated HD and non-diseased iPSCs into functional cortical neurons. While HD patient iPSCs can successfully differentiate toward a cortical fate in culture, the resulting neurons display altered transcriptomics, morphological and functional phenotypes indicative of altered corticogenesis in HD.

INTRODUCTION

Huntington's disease (HD) is an autosomal-dominant neurodegenerative disease caused by an expanded CAG trinucleotide repeat within the first exon of the Huntingtin (*HTT*) gene, with the number of repeats inversely correlated to age of onset and severity (HDCRG, 1993; Duyao et al., 1993, Andrew et al., 1993). The devastating symptoms of HD include progressive motor dysfunction, chorea, cognitive impairment, psychiatric abnormalities and, ultimately, death (Vonsattel et al., 2008). The HTT protein is ubiquitously expressed and has global roles in apoptosis (Hickey and Chesselet, 2003), yet mutant Huntingtin (mtHTT) primarily leads to the dysfunction and death of striatal medium spiny neurons and subsequently cortical projection neurons (Macdonald and Halliday, 2002; Thu et al., 2010). Interestingly, neuronal dysfunction starts years before overt clinical symptoms, including reduced cortico-striatal functional connectivity (Unschuld et al., 2012) and cortical white matter atrophy (Fennema-Notestine et al., 2004; Rosas et al., 2010). HD mouse models also display several early changes, including altered cortical cell migration and electrophysiological properties, as well as reduced cortical thickness (Cummings et al., 2006, 2007, 2010; Stern, 2011; Molina-Calavita et al., 2014; Barnat et al., 2017).

HD studies have primarily focused on neurodegeneration occurring in adulthood. However, changes in cerebral cortex development (corticogenesis) have also been implicated (Molina-Calavita et al., 2014; McKinstry et al., 2014; Molero et al., 2009, 2016). This may be related to the role of HTT in cortical progenitor spindle orientation during mitosis (Godin et al., 2010; Tong et al., 2011). Spindle orientation is critical to corticogenesis, as the cleavage plane during cell division regulates the daughter cell fate (Gauthier-Fisher et al., 2009; Marzesco et al., 2009). Htt-depleted animal models display altered migration of progenitors into the developing cortex, which leads to mislocalized neurons within the cortical layers (Barnat et al., 2017) and a reduction in overall cortical thickness at both the embryonic and postnatal stages (Molina-Calavita et al., 2014; Barnat et al., 2017). The necessity for Htt expression is mirrored in chimeric mice, in which cells with a complete knockout of Htt were able to generate neurons throughout the brain but were much sparser than predicted in the cerebral cortex and striatum (Reiner et al., 2001), pointing to the necessity for Htt function in the neurodevelopment of neurons in these regions. Also, when Htt levels were reduced, massive neurodevelopmental phenotypes could be seen (White et al., 1997; O'Kusky et al., 1999). Alterations in morphology also occur within cortical neuron dendrites (Barnat et al., 2017; McKinstry et al., 2014). Together, this implicates HTT in the regulation of cortical layering and the early migration and dendritic morphogenesis of cortical neurons. These neurodevelopmental roles of HTT support an altered brain development, which may account for the smaller intracranial adult brain volume (Nopoulos et al., 2010) and smaller head size (Lee et al., 2012) that occur in HD carriers decades before predicted onset.

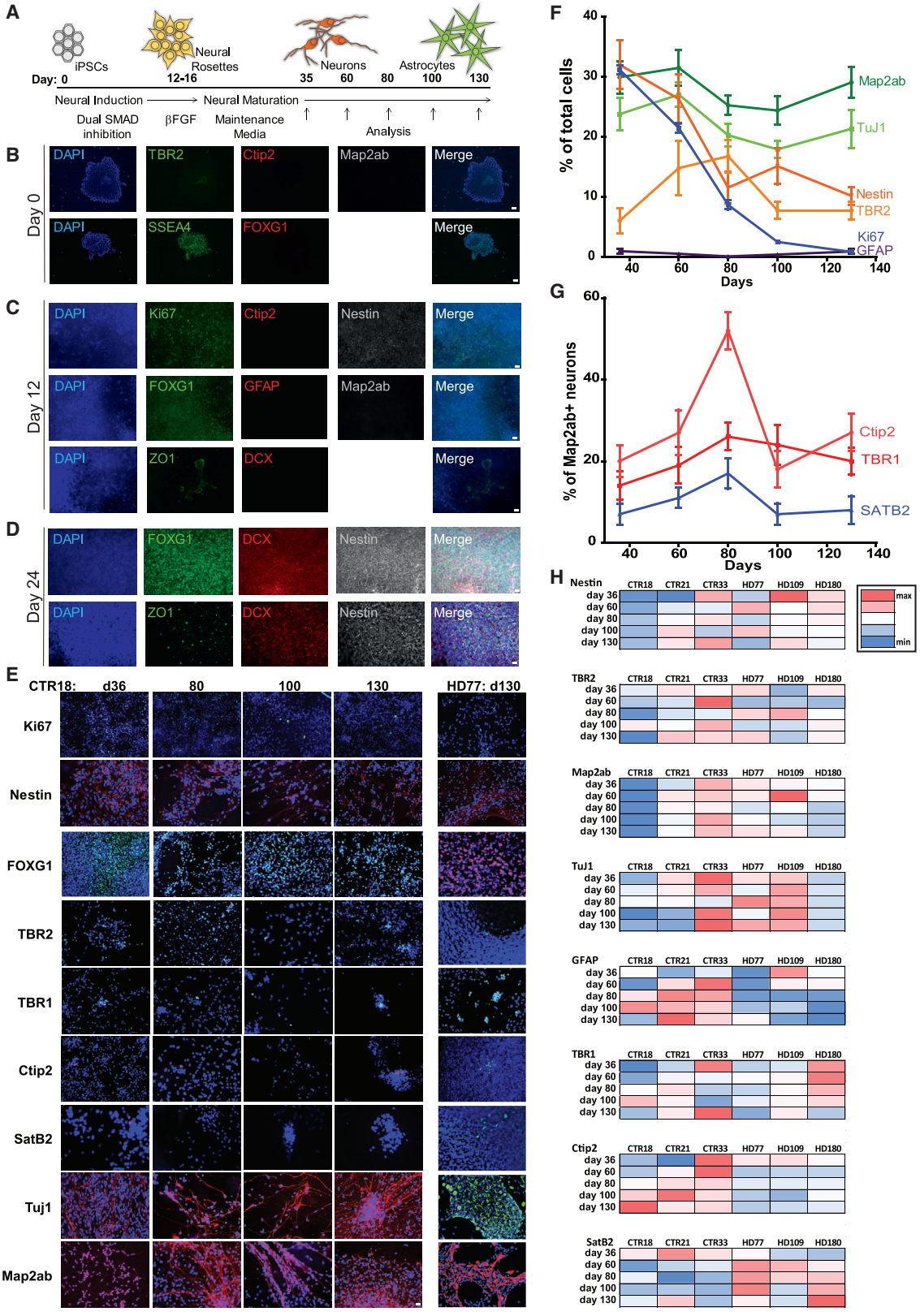

(legend on next page)

Rodent models of HD have helped to further understand HD and the role of development; however, the rodent central nervous system has fundamental differences compared to humans (Dolmetsch and Geschwind, 2011; Clowry et al., 2010). The altered corticogenesis in HD murine models may recapitulate what has been tangentially described in humans, but this has not been confirmed due to a lack of embryonic/fetal cortical HD tissue. Fortunately, human-based models are now possible with induced pluripotent stem cells (iPSCs), somatic cells reprogrammed to a pluripotent state with the capacity to generate any cell in the body (Takahashi and Yamanaka, 2006; Magnuson et al., 1982). We have shown that HD-patient-derived iPSCs, upon differentiation into a striatal fate, display an altered neurodevelopmental phenotype (Mattis and Svendsen, 2017; HD iPSC Consortium, 2012, 2017). Although striatal pathology has been extensively studied, the cortical contribution to HD remains underinvestigated. The mature human cortex is composed of six layers, with neurons in development first forming the deep layers (V and VI) and subsequently born neurons migrating past the deep layer neurons to form the upper (II–IV) cortical layers. Human iPSCs can be differentiated into a cerebral cortical fate with distinct markers of either the deep layer or upper layer neurons, and their development recapitulates the timing of *in vivo* corticogenesis (Shi et al., 2012).

Here, iPSC lines from patients with juvenile-onset HD (180, 109, or 77 CAG repeats) were differentiated toward a cortical fate using an established protocol in order to examine the role of an expanded CAG repeat on corticogenesis. The HD iPSCs generated deep and upper layer cortical neurons along the same timeline and in similar quantities as control iPSCs (33, 21, or 18 CAG repeats), but the HD cortical cells, compared to control, showed distinct differences in gene expression, many overlapping with those detected in the BA4 motor cortical region of postmortem HD brains. Transcriptomics indicated both delayed maturation and altered morphology of the HD cortical neurons, which were substantiated with electrophysiology and neurite measurements. This report provides evidence of altered corticogenesis in human HD patient tissues, which is critical for understanding initial contributors to HD and developing potential early treatment regimes.

RESULTS

Differentiation of HD and Control iPSCs toward a Cerebral Cortical Fate

HD (180, 109, and 77 CAGs) and control (CTR; 33, 21, and 18 CAGs) iPSC lines were generated and characterized as previously described (Mattis et al., 2015). All lines were differentiated from their pluripotent state into a cerebral cortical fate using a published protocol (Shi et al., 2012) (Figure 1A). Dual SMAD inhibition was used to differentiate iPSCs from their SSEA4$^+$ pluripotent state (negative for the neural markers FOXG1, TBR2, Ctip2, and Map2ab) (Figure 1B) toward ZO1$^+$ neural rosettes by day 12 of differentiation (Figure 1C). At this point, the cells also positive for markers of dividing cells (Ki67) and early neural progenitors (Nestin) and faintly expressed markers of forebrain (FOXG1), but not more mature neural markers (Ctip2, GFAP, and DCX). To further promote a neuroepithelial fate, βFGF was added for 2 days, after which time cells were almost entirely a sheet of FOXG1$^+$, Nestin$^+$, and DCX$^+$ committed forebrain progenitors (Figure 1D). These cells were then plated on coverslips, placed in a neuronal maturation media, and assayed for markers of cortical development and commitment to a mature neuronal fate by nonbiased stereological counting on days 36, 60, 80, 100, and 130 of differentiation (Figures 1E and S1). Counts of specific populations demonstrate that these populations appear over a developmentally appropriate time course for both HD and control lines. Progenitor cells (Nestin$^+$) and dividing cells (Ki67$^+$) decrease over the course of 36–130 days, going from ~30% of cells expressing these markers to ~10% and 1%, respectively (Figures 1E and 1F). However, by day 36, general neuronal markers (Map2ab and TuJ1) are already ~25%–30% of all cells and maintain their expression over the duration of the 130 days (Figures 1E and 1F), as do specific deep layer (Ctip2 and TBR1, ~20% of neurons) and upper layer (SatB2, ~10%) (Figures 1E and 1G) cortical markers. As reported previously (Shi

Figure 1. Immunocytochemistry Revealed that HD (HD180, HD109, and HD77 CAG) and Control (CTR33, CTR21, and CTR18 CAG) iPSCs Can Differentiate into a Population of Cerebral Cortical Progenitors, Neurons, and Glia in a Developmentally Appropriate Time Course

(A) Schematic of cortical differentiation timeline from day 0 (iPSC colonies) to day 130 (mature cortical neurons and glia).

(B) Feeder-free iPSC colonies express markers of pluripotency (SSEA4) but do not express markers of a committed neuronal or cortical fate (FOXG1, TBR2, Ctip2, and Map2ab).

(C) By day 12 of differentiation, cells are dividing neural progenitors (Ki67 and Nestin), which are beginning to form neural rosettes (ZO1), and while they are beginning to express FOXG1, they are not yet fully committed to a neuronal or cortical fate (Ctip2, GFAP, Map2ab, and DCX negative). Images displayed are CTR21 but are representative of all lines.

(D) By day 24 of differentiation, the cultures are almost an entirely pure sheet of FOXG1-expressing neural rosettes (ZO1, DCX, and Nestin). Images displayed are CTR21 but are representative of all lines.

(E) Representative images across the time course of expression of differentiation from days (d) 36 to 130 of differentiation of dividing neural progenitors (Ki67 and Nestin), commitment to a cortical progenitor fate (FOXG1), cortical progenitors (TBR2), deep layer cortical neurons (TBR1 and Ctip2), upper layer neurons (SatB2), and general markers of neurons (TuJ1 and Map2ab). Images displayed are CTR18 but are representative of all lines. On the right, images of the HD77 line at the 130-day time point.

(F) Graphs of overall (HD and control) glia (dark purple), radial glia (light purple), neurons (green), and cells with a committed cortical fate (orange) counts over the course of 130 days of differentiation.

(G) Graphs of overall deep layer neuron (red) and upper layer neuron (blue) counts over the course of 130 days of differentiation.

(H) Heatmap of the relative *Z* score of counts for each marker within each cell line over the course of 130 days of differentiation. All images were taken with a 20× objective (scale bar indicates 25 μm).

Data are presented as mean ± SEM. All cell counts were from at least three separate differentiations. Please see STAR Methods for statistical information. See also Figure S1.

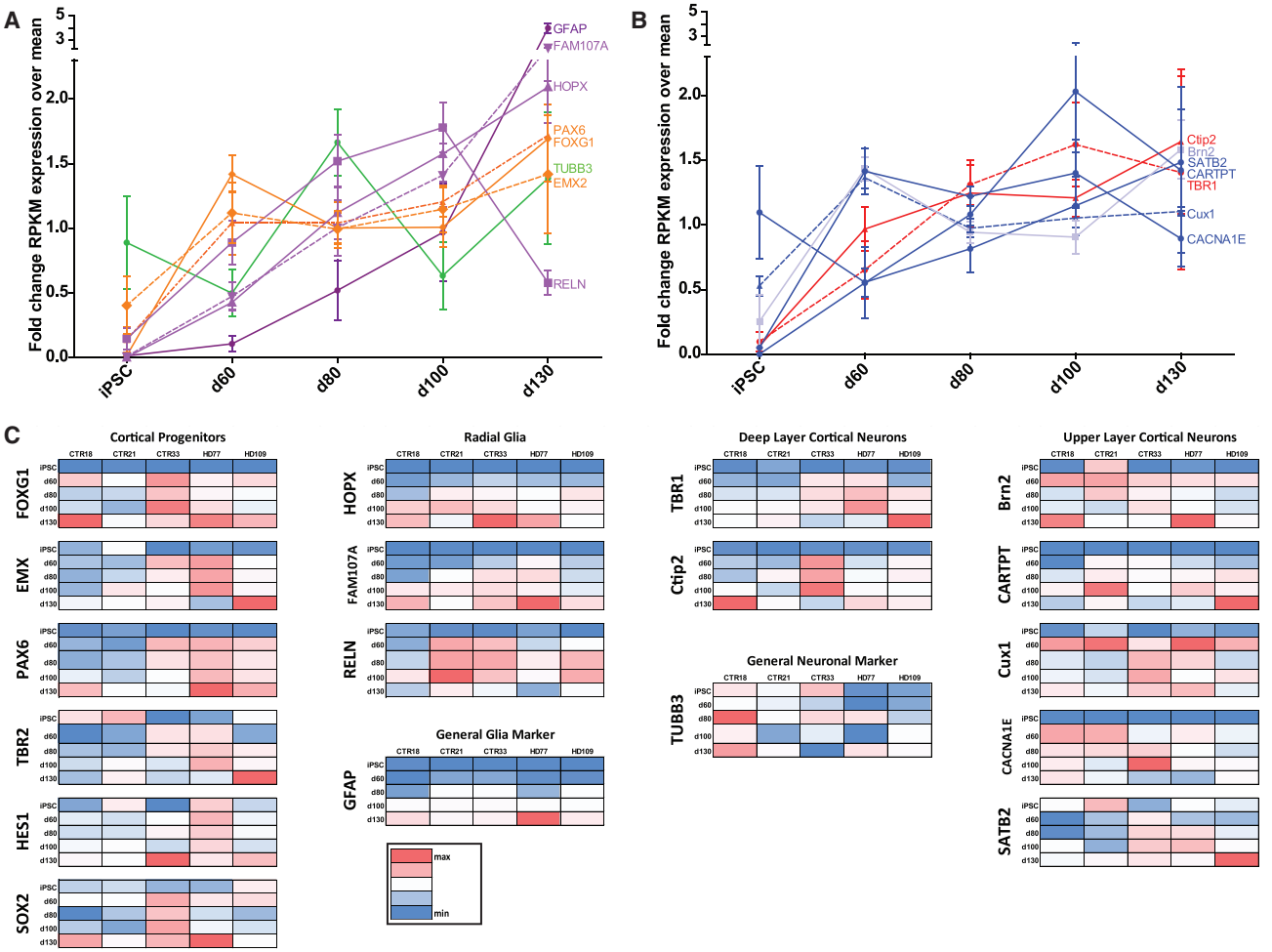

Figure 2. Transcriptomic Analysis Also Revealed Cortical and HD iPSC Differentiation toward a Cortical Fate

(A) Graphs of overall reads per kilobase million (RPKM) values of HD (109 and 77 CAGs) and control (33, 21, and 18 CAGs) glia (dark purple), radial glia (light purple), neurons (green), and cells with a committed cortical fate (orange) at time points (day [d] 0 [iPSC stage], 60, 80, 100, and 130) over the course of 130 days of differentiation.

(B) Graphs of overall (HD and control) RPKM values of deep layer neuron (red) and upper layer neuron (blue), over the course of 130 days of differentiation.

(C) Heatmap of the relative *Z* score of RPKM values for each marker within each cell line over the course of 130 days of differentiation (time points: day [d] 0 [iPSC stage], 60, 80, 100, and 130 of differentiation). Gene expression is shown by color intensity in a red-to-blue spectrum, where upregulated genes are shown in red and downregulated genes are shown in blue (gray indicates absent sample). Genes are divided into categories of cortical progenitors (FOXG1, EMX, PAX6, TBR2, HES1, and SOX2), radial glia (HOPX, FAM107A, and RELN), glia (GFAP), deep layer cortical neurons (TBR1 and CTIP2), neurons (TUBB3), and upper layer cortical neurons (Brn2, CARTPT, Cux1, CACNA1E, and SATB2).

Please see STAR Methods for statistical information.

et al., 2012), the presence of a GFAP$^+$ glial population of cells was very low (only ~2%), rising only after ~100 days in culture (Figure 1F). There is no significant effect seen in the percentages of cells produced of any one marker assayed between the HD and control lines (Figures 1H and S1).

RNA sequencing recapitulates the stereology data from samples at days 0 (iPSC colony stage), 60, 80, 100, and 130 of differentiation (Figure 2). By day 60, increased expression of committed forebrain markers such as FOXG1 is seen, in addition to expression of known transcriptional regulators of the neocortex (EMX2 and PAX6; Figures 2A and 2C). Transcripts of radial glia populations (HOPX, FAM107A, and RELN; Figures 2A and 2C) were seen from day 60 (the first time point analyzed) onward. Neuronal gene expression (TUBB3; Figures 2A and 2C), as well as specific cerebral cortex layer transcripts (deep layers: TBR1 and Ctip2; upper layers: Cux1 and CACNA1E; Figures 2B and 2C), is also seen from day 60 onward. Interestingly, the upper layer cortical transcript CARTPT was not detected until day 100 of differentiation (Figures 2B and 2C), in line with *in vivo* corticogenesis patterns. In addition, GFAP transcripts were greatly upregulated by 130, in agreement with the immunocytochemistry marker counts (Figures 2A and 2C). These transcripts did not significantly differ between HD and controls.

A

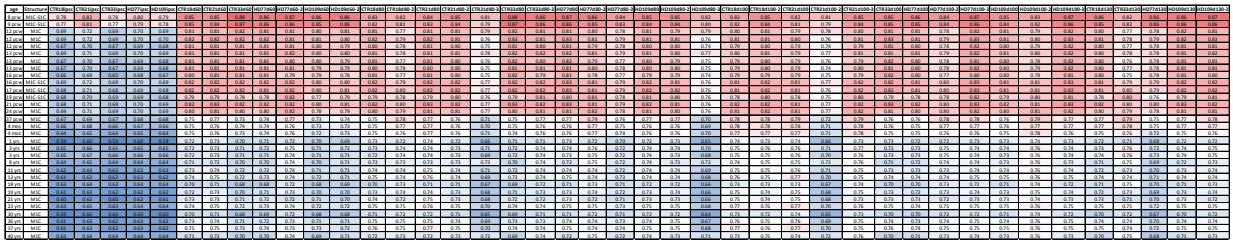

B

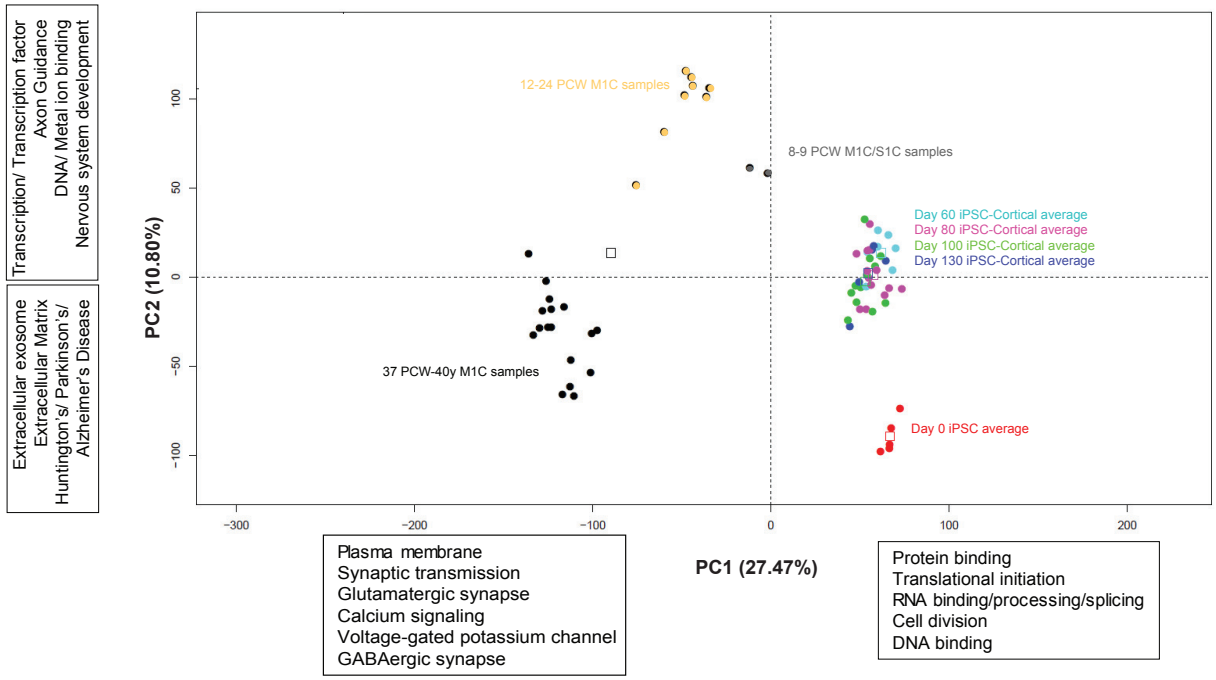

C

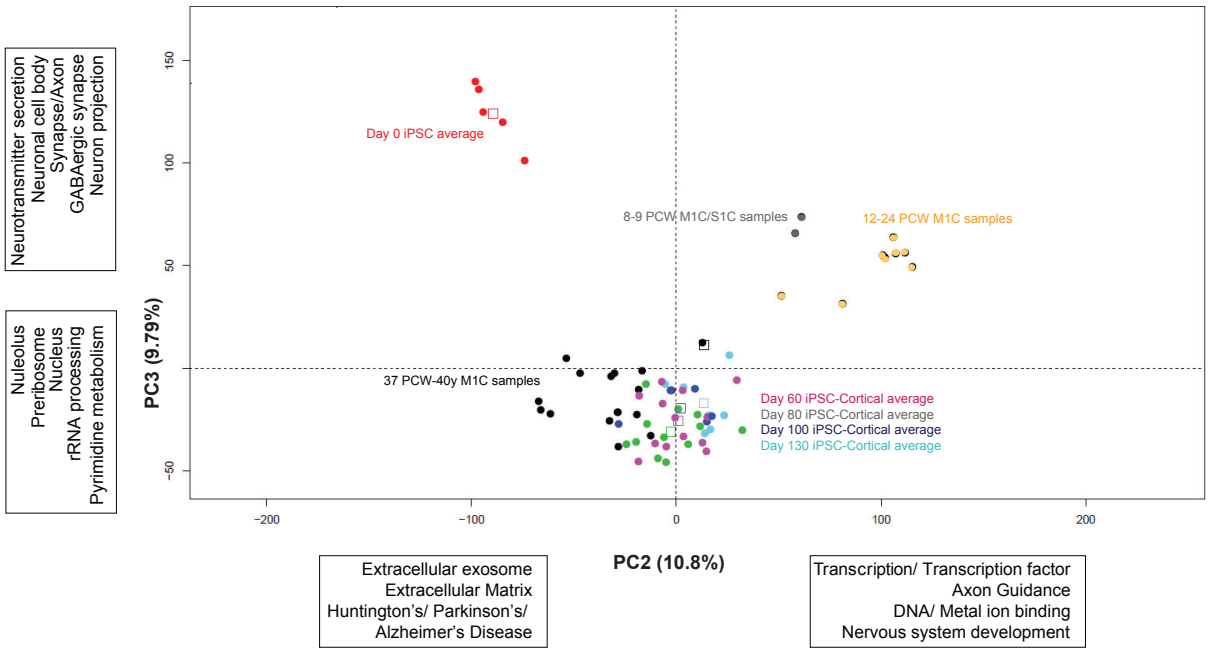

(legend on next page)

In order to validate the developmental paradigm of the *in-vitro*-derived cortical samples, their transcriptomic profiles were compared to that of the developing motor cortex from 8 post-conception weeks (PCW) to 40 years of age (Allen Brain Institute; Handel et al., 2016) using Pearson correlation (Figure 3A; Table S1). The iPSC-derived cortical samples were shown to be fetal in nature, most significantly correlating with that of the 8–9 PCW primary motor-sensory cortex (Figure 3A; Table S1). To further address the developmental profiles of the *in-vitro*-derived cortical samples compared to the *in vivo* motor cortex, principal-component analysis (PCA) was performed. Principal components (PCs) 1–3 reveal that the iPSC-derived cortical samples from day 60 to 130 of differentiation grouped away from the iPSCs and toward a motor cortical fate (Figures 3B and 3C). Gene ontology (GO) enrichment was used to gain a better biological understanding of these PCs (HD iPSC Consortium, 2012). On the PC1 axis (Figure 3B, x axis), the iPSCs were in the positive coordinates, defined by GO terms indicative of replicating cells, such as "cell division." The iPSC-derived cortical neurons were between the iPSCs and the developing motor cortex, which continued in trajectory toward the increasing negative PC1 coordinate with *in vivo* development, defined by GO terms associated with a mature neuronal network. Hierarchical clustering of log2-transformed gene expression values showed a demarcation in PC1 between the *in vitro* and *in vivo* samples (Figure S2). On the PC2 axis (Figure 3B, y axis), the earlier-time-point iPSC-derived cortical neurons generally mapped to the positive coordinate with the 8–24 PCW motor cortex, as defined by GO terms associated with "nervous system development," while the later time points mapped toward the negative coordinates with the post-natal and adult motor cortex and were defined by terms describing adult neurodegenerative disorders, including HD. On the PC3 axis (Figure 3C, y axis), the iPSC-derived cortical neurons were mapped to the negative coordinate with the 37 PCW to 40 year motor cortex, defined by terms associated with cellular maintenance, such as "rRNA processing." Upon hierarchical clustering of PC2 and PC3, the iPSC-derived cortical cells clustered away from the undifferentiated iPSCs and with the developing motor cortex (Figures S2B and S2C). In PC2, it was noted that the iPSC-derived cortical cultures also tended to group by repeat length, with a distinction seen in the dendrogram.

Together, this demonstrates that both HD and control iPSCs can be differentiated toward a cortical cell fate that is most similar to the early fetal cerebral cortex. There was not a significant difference between the generation of either deep or upper layer cortical neurons, as demonstrated by heatmap (*Z* score; Figure 1G) or raw percentage counts (Figure S2), in concordance with HTT-depleted or HD mice (Molina-Calavita et al., 2014; Barnat et al., 2017). However, significantly differentially expressed marker genes, such as GFAP (Figure 1J), demonstrate that potentially more subtle differences were likely present in these cultures.

HD iPSC-Derived Cortical Neurons in 2D Display Transcriptomic Profiles Reflective of Altered Neuronal Development

When PCA was performed on the whole-transcriptome analysis of the HD (77 or 109 CAGs) and control (18, 21, or 33 CAGs) iPSC-derived cortical samples in the absence of *in vivo* motor cortex, at all time points (days 0, 60, 80, 100, and 130 of differentiation), the HD samples largely segregated independently from controls (Figure 4A). This is also reflected in the hierarchical clustering, in which the HD and control samples had a clear distinction on the dendrogram (Figure S3), demonstrating the transcriptomic variation between the disease and control states.

To further investigate the variability between HD and control cultures, differentially expressed genes (DEGs; Table S3) were examined at all time points. Ingenuity Pathway Analysis (IPA) was used to examine the potential biological implications of the DEGs on the disease process (Table S2; Figure 4). At the iPSC stage (day 0), the DEGs between HD and controls can largely be described by the "top diseases and functions" networks associated with cellular proliferation and development (Table S2). However, by days 60, 80, and/or 100 of differentiation, the top categories describing the HD gene expression changes were associated with cellular morphology, cell movement, hereditary disorder, neurological disease, and nervous system development and function (Table S2).

For example, network 4 at 100 days of differentiation highlights that in the HD samples, genes associated with voltage-gated sodium currents (SCN1A, SCN2A, SCN4B, and SCN9A) were largely downregulated in the HD samples (Table S2, bold; Figure 4B, green). As voltage-gated sodium currents are obviously essential to the ability for neurons to generate a functional action potential, the decreased expression of these genes could potentially be indicative of a delayed maturation phenotype in the cortical cultures, as has been previously described in HD iPSC-derived models of the developing striatum (Mattis et al., 2015; HD iPSC Consortium, 2012, 2017; An et al., 2012). These pathways have also been previously implicated in neurodegenerative disease, and furthermore, specifically in HD (Neueder and Bates, 2014).

Figure 3. iPSC-Derived Cortical Cultures Correlate with the *In Vivo* Fetal Brain

(A) Pearson correlation of the developing motor cortex from the Allen Brain Institute (8–9 post-conception weeks [PCW] to 40 years of age) to the iPSC-derived cortical cultures (days 0, 60, 80, 100, and 130 of differentiation). Red indicates high correlation of the samples to brain regions, while blue indicates a lesser correlation. The highest correlation between each *in vitro* and *in vivo* cortical sample is highlighted by a bold outline.

(B) Principal-component analysis (PCA) of the top 500 genes of developing motor cortex (8–9 PCW [green], 12–24 PCW [black], or 37 PCW to 40 years of age [red]) and both control and HD iPSC-derived cortical samples (days 0 [gold], 60 [magenta], 80 [gray], 100 [dark blue], and 130 [light blue] of differentiation) and gene ontology (GO) terms that define the top 1,000 genes of the negative and positive axes of dimension (Dim) 1–2.

(C) PCA of the developing motor cortex and iPSC-derived cortical samples and GO terms that define the top 1,000 genes of the negative and positive axes of Dim 2–3.

Please see STAR Methods for statistical information. See also Table S1 and Figure S2.

A

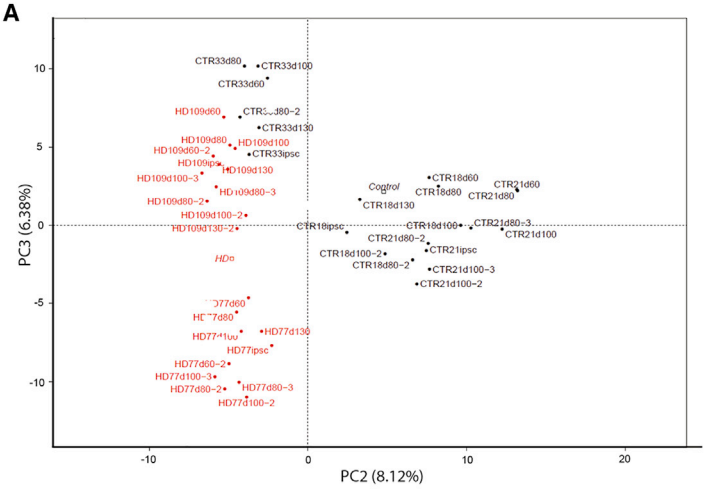

B iPSC-derived Cortical Neurons, day 80: Network 4

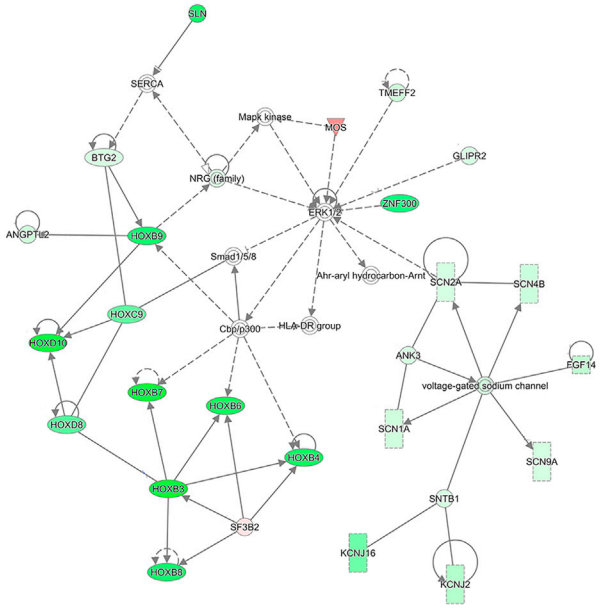

C **Day 100 iPSC-derived cortex overlap with BA4 HD patient cortex**

ID	Top Diseases and Functions	Molecules in Network	Score
1	Hereditary Disorder, Neurological Disease, Organismal Injury and Abnormalities	**SPON1, ST8SIA1,** Tgf beta, **PCSK1, PCSK2,** PDGF BB, Pka, **PKIA,** Proinsulin, **RAB31, RGS4, RYR3, SLC7A11,** ERK1/2, FSH, **HMGCS1, ITPR2,** LDL, Lh, Mapk, Mek, **MT1X, MT2A, NEFL, NTRK2, AGT,** Alp, Ap1, **BBOX1,** Calcineurin protein(s), CaMKII, Cg, Creb, **DUSP6, ELK1**	49
2	Amino Acid Metabolism, Molecular Transport, Small Molecule Biochemistry	**SLC17A7,** SLC17A8, SRF-ELK1, TP53, **TULP3,** ZNF839, ZNF385B, NECAB3, OCIAD2, OMG, PGLYRP2, POMZP3, Ppp1r15a, RAB26, **SESN1,** SH3BGRL2, FOS, **GPM6B, H2AFJ,** IFNG, isopropyl alcohol, **KCNAB3,** MAPK3, MPV17L, **NEBL, ALDH1L1,** APP, ARAP2, BDNF, C1orf116, CARF, CDH1, CMTM8, FAM126B, **FGF14**	19
3	Cellular Growth and Proliferation, Cell Cycle, Cell Morphology	SHP2-PI3K-GAB2, TRAF1-TRAF2-TRAF3, Vegf, Vegfr dimer, ZNF675, **NRG1,** P38 MAPK, PI3K (complex), Pkc(s), **PON2,** Prl4a1, Rac, RAS, RNU7-1, miR-9-3p (and other miRNAs w/seed UAAAGCU), **MT1E, MT1G,** MUC8, NFkB (complex), Histone h4, **HSPB8,** IkB-NfkB, Insulin, Jnk, **KAT2B, ACLY,** Akt, ANGPTL1, BANCR, BCAR4, DBH-AS1, Erbb3 dimer, ERK, Hdac, Histone h3	14

(legend on next page)

Additionally, at several time points (Table S2: day 60, network 1; day 80, network 2; day 100, networks 1, 2, and 6), the genes involved with collagen formation and proper cellular morphology were downregulated in HD. There have been previous implications of altered cellular adhesion and morphology in HD (Reis et al., 2011), and this may be reflective of similar findings in the iPSC-derived cortical neurons.

In order to compare the DEGs from the iPSC-derived HD cortical cultures to the patient condition, we next used IPA to analyze the DEGs from a previously published transcriptomic dataset from the Brodmann area 4 (BA4) motor cortex of postmortem HD patients, as compared to controls. Using the GEO2R platform with Benjamini-Hochberg false discovery rate (FDR) correction, 953 DEGs were found between HD and non-diseased BA4 regions of the cerebral cortex from this dataset. These DEGs revealed similarly affected network functions to the *in vitro* cortical samples at 60, 80, and 100 days of differentiation, including Developmental or Hereditary Disorder. Although these samples are from a broad range of samples (Vonsattel grade 0–3), within the BA4 HD patient samples, there was only one DEG between the grade 0–1 and 2–3 samples (SLC9A3R2). Therefore, all HD BA4 postmortem samples were grouped together to compare to the iPSC-derived HD cortical samples. When examining the overlap of the day 100 *in vitro* iPSC-derived cortical neuron DEGs with the *in vivo* human patient DEGs (Figures 4C and S4), there was some conserved gene dysregulation that can be generally classified in networks describing neurological disease, together adding further validity that a developmental model can capture elements of the patient condition.

Weighted gene co-expression network analysis (WGCNA) was then used to link tightly co-expressed gene modules to known traits (Figure 5A; Langfelder and Horvath, 2008; Zhang and Horvath, 2005). 23,106 genes across the iPSCs and iPSC-derived cortical samples were hierarchically clustered based on topological overlap (Figure 5B). This analysis identified 42 modules, which are arbitrarily associated with colors. The genes within those modules were then evaluated for correlation with "traits" of the differentiations, namely "day of differentiation" and "HD" (Figure 5C). The turquoise, purple, light green, gray 60, dark olive green, tan, and light yellow modules were found to be anti-correlated with the trait "days of differentiation" (Figure 5C). These modules can be defined by biological terms describing cell components (e.g., plasma membrane, cytosol, nucleoplasm, nucleolus, mitochondrion, and nucleus) and cellular functions (e.g., spliceosomal assembly, DNA replication, and protein sumoylation or transport). The blue, brown, salmon, red, light cyan, midnight blue, yellow, dark magenta, violet, green, steel blue, pink, and saddle brown modules are significantly correlated with days of differentiation. These modules also describe not only cellular components (plasma membrane, cytoplasm, and centriole) but also terms associated with a neuronal network (synapse, presynaptic membrane, voltage-gated potassium channel, axon guidance, neuron projection, and nervous system development). This validates the PCA findings that the iPSCs are differentiating to a neural network upon differentiation.

Two modules were significantly correlated to the trait "HD": gray and dark orange (Figure 5C). However, as the gray module (anti-correlated to HD) consists of genes that do not fall into a true module, only the genes associated with dark orange (correlated with HD) were evaluated for their biological relevance. GO analysis identified biological terms associated with "nucleoplasm," "protein binding," "cytosol," and "mitochondrion" (Figure 5D). The biological terms that define this module largely describe cellular components, similarly to those describing modules anti-correlated to days of differentiation. In part, this validates previous findings of IPA examination of the DEGs, which indicated potential issues with maturation.

HD iPSC-Derived Cortical Neurons in 2D Display Measurable Phenotypes in Neurite Morphology

Transcriptional profiles implicating altered cellular morphology in the HD iPSC-derived cortical cultures is in line with previous publications, which demonstrated that Htt is responsible for cortical neuronal polarity (Barnat et al., 2017). Therefore, the morphology of the iPSC-derived cortical Map2ab$^+$ neurons was examined at day 130 of differentiation. In order to first assess overall morphology, the neurons were categorized as unbranched, branched, or multipolar (Figure 6A), and each morphological type was counted (Barnat et al., 2017). Overall, there was no difference in the percentage of Map2ab$^+$ neurons displaying differing morphology between the HD iPSC-derived cortical neurons and those from controls (Figure 6B).

As the importance of wild-type Htt during corticogenesis has been described for proper dendritic development in cortical neurons (Barnat et al., 2017), neurite length was assessed in the day 130 HD cortical cultures. Map2ab$^+$ neuronal outgrowths were measured using Neuroleucida tracing software (Figure 6C). Not only did controls generally demonstrate higher mean neurite lengths than the HD neurons (Figure 6D; $p = 0.0474$), but there was a significant effect of the CAG repeat length across the entire series of both control and HD neurons ($p < 0.0001$, $r = -0.7698$), where increased CAG repeat length correlated directly with decreased neurite lengths. These CAG-repeat-length-dependent cortical changes in controls have been previously described in school-aged children within the "normal" CAG length range (Lee et al., 2017). Together, while

Figure 4. Transcriptomic Differences Seen between HD and Control Demonstrates Some Overlap with Those Seen in HD BA4 Motor Cortex Post-mortem Samples

(A) PCA demonstrates clear differences between HD and control samples at the different stages of cortical differentiation from day 0 to day 130.

(B) Network 4 altered in HD samples at day 80 is mapped. Green genes are significantly downregulated in HD samples, while red genes are upregulated.

(C) The greatest degree of DEG overlap between *in vitro* and *in vivo* (BA4 samples; yellow) samples occurs at day 100 of differentiation. IPA groups these 35 overlapping genes into pathways representing neurological disease and cell morphology. Bold genes are those within the network that are found in the overlapping DEGs of day 100 and the BA4 cortex.

Please see STAR Methods for statistical information. See also Tables S2 and S3; Figures S3 and S4.

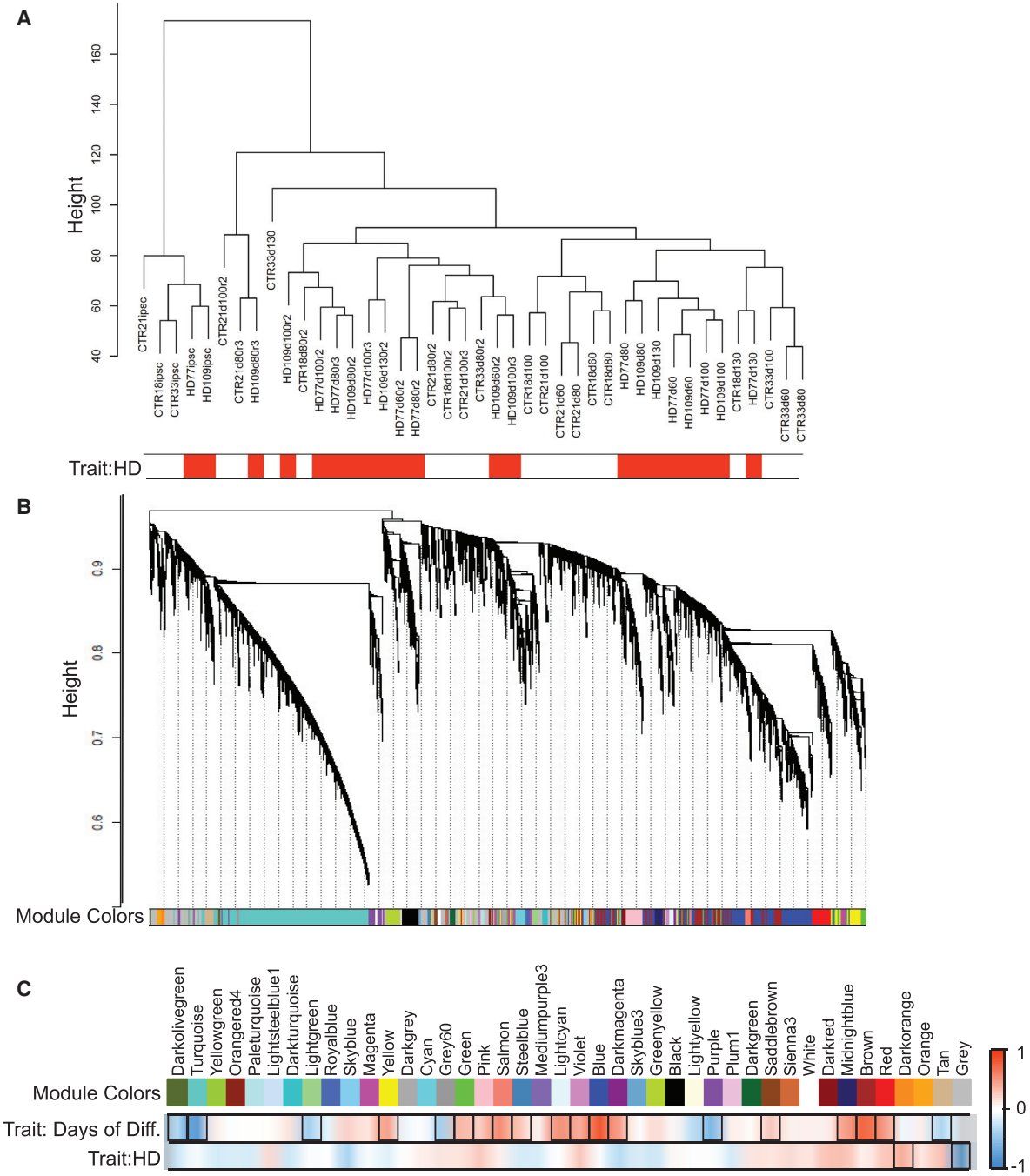

D

Term	Genes	Adj. P Value
GO:0005654~nucleoplasm	PSMB10, MMS19, AURKAIP1, MAPKAPK5, LSM7, NR2C2AP, BANF1, RPS19BP1, DDX47, C12ORF10, PRMT5, SNF8, MED27, HNRNPC, NUDC, DDX39A, GARS, FDPS, SNW1, ZNF143, SMN2, TAF11, POLD4, CCDC51, PRELID1, ATF4, BRMS1, PPP1R8, UROD, HNRNPH1, NHP2	0.004168576
GO:0005515~protein binding	MMS19, TSPO, C19ORF73, AURKAIP1, ATP5B, LSM7, NR2C2AP, RASSF7, RPS19BP1, EIF4EBP3, TRAPPC6A, GSTM4, PRMT5, MED27, SERTAD3, IMPDH2, CCDC28A, DDX39A, RAMP2, CHAC1, VTI1B, ZNF143, SMN2, TAF11, EEF1G, PEBP1, PLLP, PELO, UROD, NHP2, PSMB10, ECH1, DBNDD2, MRPS12, MAPKAPK5, FKBP1B, HSCB, BANF1, ANXA7, EIF3D, DDX47, ECE2, BUD13, AKR1A1, RAC3, SNF8, TBC1D7, EIF3I, HNRNPC, NUDC, FKBPL, SERGEF, LAMTOR1, TSR2, SNW1, PRELID1, POLD4, ATF4, BRMS1, PPP1R8, RNF5, ENDOG, ATP2A1, BOLA1, HNRNPH1, SSNA1, PDCD6	0.00524401
GO:0005829~cytosol	RPL18, PSMB10, GMPR2, NARS, MAPKAPK5, LSM7, FKBP1B, BANF1, TRAPPC6A, EIF3D, ANXA7, GSTM4, AKR1A1, RAC3, PRMT5, PGAM4, SNF8, EIF3I, HNRNPC, IMPDH2, NUDC, MARS, FKBPL, CHAC1, GARS, FDPS, VTI1B, SMN2, ENDOG, PEBP1, EEF1G, UROD, SSNA1	0.009085533
GO:0005739~mitochondrion	TSPO, ECH1, AURKAIP1, NARS, MRPS12, ATP5B, MRPS24, HINT2, FDPS, HSCB, CCDC51, PRELID1, C12ORF10, ENDOG, ATP2A1, ALKBH1, BOLA1, SLC25A26	0.017877546

(legend on next page)

no differences were seen in overall branching morphology, these data validate the transcriptomic results of a CAG-length-dependent change in iPSC-derived cortical neuronal morphology.

HD iPSC-Derived Cortical Neurons in 2D Display Measurable Phenotypes in Electrophysiology

The transcriptomic analysis also indicated a possible delay in functional maturity, with a specific downregulation of voltage-gated sodium channels (Table S2; Figure 4B). Therefore, in order to investigate a potential phenotypic effect of these alterations, both spontaneous and induced action potentials were examined in the HD iPSC-derived cortical neurons. First, multielectrode array (MEA) was used to track the spontaneous activity in control and HD cultures in over an extended differentiation timeline (weekly from day ~30 to 200+). Over this time course, the control neurons were not only more likely to be active than HD neurons, as measured by percentage of wells to have spontaneous activity ($p = 0.0049$; Figures 7A and 7B), but also had greater activity, as measured by increased spontaneous firing events within the wells ($p = 0.0054$; Figures 7C and 7D). Interestingly, in both measurements, there is a significant effect of repeat count ($p = 0.0103$ for Figures 7A and 7B and $p < 0.0001$ for Figures 7C and 7D, respectively), again identifying a CAG-repeat-length-dependent phenotype. Also, a stronger effect of the repeats is seen at the earlier time points, as the HD neurons did not begin to reliably spontaneously fire action potentials until 15 weeks of differentiation, whereas the control neurons fired from the earliest time points examined (5 weeks). This implicates a potential delay in the functional maturation of the HD cortical neurons.

In order to further validate this potential delay in maturation, single-cell patch-clamp electrophysiology was performed on the HD and control iPSC-derived cortical cultures. At 60 days of differentiation, there was no significant difference between the percentages of HD or control iPSC-derived cortical neurons in the populations that were able to fire an induced action potential (Figure 7E), as the neurons assessed at this time point were mostly relatively immature and firing was lower across the board. This immaturity was defined by the relatively high mean resting membrane of all cells (around −30 mV) (Figure 7F). However, by 80 days of differentiation, the control iPSC-derived cortical neurons had significantly matured, as measured by a decreased mean resting membrane potential (around −45 mV) (Figure 7F). Consequentially, an increased percentage of neurons were able to generate an induced action potential, with some even producing trains of action potentials, indicating that these neurons had matured over the 20 additional days of differentiation (Figure 7E). However, during this time, the HD lines did not demonstrate a decreased resting membrane potential and therefore did not increase the percentage of cells able to generate an action potential. Together, this validates the potential delay in functional maturation of the HD cortical neurons as seen by spontaneous activity in the MEA recordings.

DISCUSSION

Altered neurodevelopment has been implicated in classically defined adult neurodegenerative diseases, such as HD (Molero et al., 2009, 2016; Mattis and Svendsen, 2017; HD iPSC Consortium, 2012, 2017; McKinstry et al., 2014; Barnat et al., 2017). HTT is intricately involved in corticogenesis (Molina-Calavita et al., 2014; Barnat et al., 2017), and mtHTT causes a loss-of-function phenotype in the developing cortico-striatal circuit (McKinstry et al., 2014). While the effects of HD on striatal cells are well documented, studies assessing the impact on corticogenesis are less common and have primarily have focused on mouse models rather than human cells. Here, human HD and control iPSCs were differentiated toward cortical neurons using a previously described differentiation paradigm, and their phenotype was compared to control non-diseased lines (Shi et al., 2012).

In agreement with a cortical Htt-depleted mouse model (McKinstry et al., 2014), HD and control cultures generated similar quantities of cortical neurons of each layer, based upon assessment of markers of cortical progenitors and upper and deep layer cortical neurons commonly used in the field. However, transcriptomic analysis revealed DEGs pointing to alterations in cellular morphology and electrophysiological potential. Upon further investigation, the HD cortical neurons had shorter neurites, which corroborated the transcriptomic results indicating altered cellular morphology. Previous studies have demonstrated that the absence of Htt expression during embryonic development causes longer and more elaborate dendritic outgrowth of layer V cortical neurons, with the opposite being true for layer II and III neurons (McKinstry et al., 2014, Barnat et al., 2017). As neurite extensions in the iPSC-derived cortical neurons were measured by expression of the pan-neuronal marker Map2ab, it will be important to next assess altered neuronal morphology in cortical-layer-specific neurons. Interestingly, the HD iPSC-derived cortical cells had downregulation of voltage-gated calcium channels, such as Scn4b, which was seen previously in HD patients (Oyama et al., 2006). These channels are necessary for neurite outgrowth and axonal fasciculation (Patino and Isom, 2010), and hence their reduction may play a role in the observed altered cellular phenotype. In the

Figure 5. Weighted Gene Co-network Analysis Reveals Co-expression Modules with HD and Days of Differentiation in the iPSC-Derived Cortical Samples

(A) Samples were first clustered via dendrogram and associated with traits such as HD.

(B) Weighted gene co-expression network analysis (WGCNA) clustered 22,106 genes across iPSCs (day 0) and cortical differentiations at days 60, 80, 100, and 130 for the HD109, HD77, CTR33, CTR21, and CTR18 cell lines, based upon similar network topology ($n = 43$ samples). A dynamic tree-cutting algorithm grouped tightly networked genes into 27 different modules (illustrated by color).

(C) Heatmap illustrates correlation of the traits HD and days of differentiation (Diff.) to each color module. Benjamini-Hochberg multiple-comparison-corrected significantly correlated trait boxes are outlined in black.

(D) GO analysis of genes associated with the dark-orange module identified biological terms associated with nucleoplasm, protein binding, cytosol, and mitochondrion. The adjusted (Adj.) p value was calculated using the Benjamini-Hochberg method.

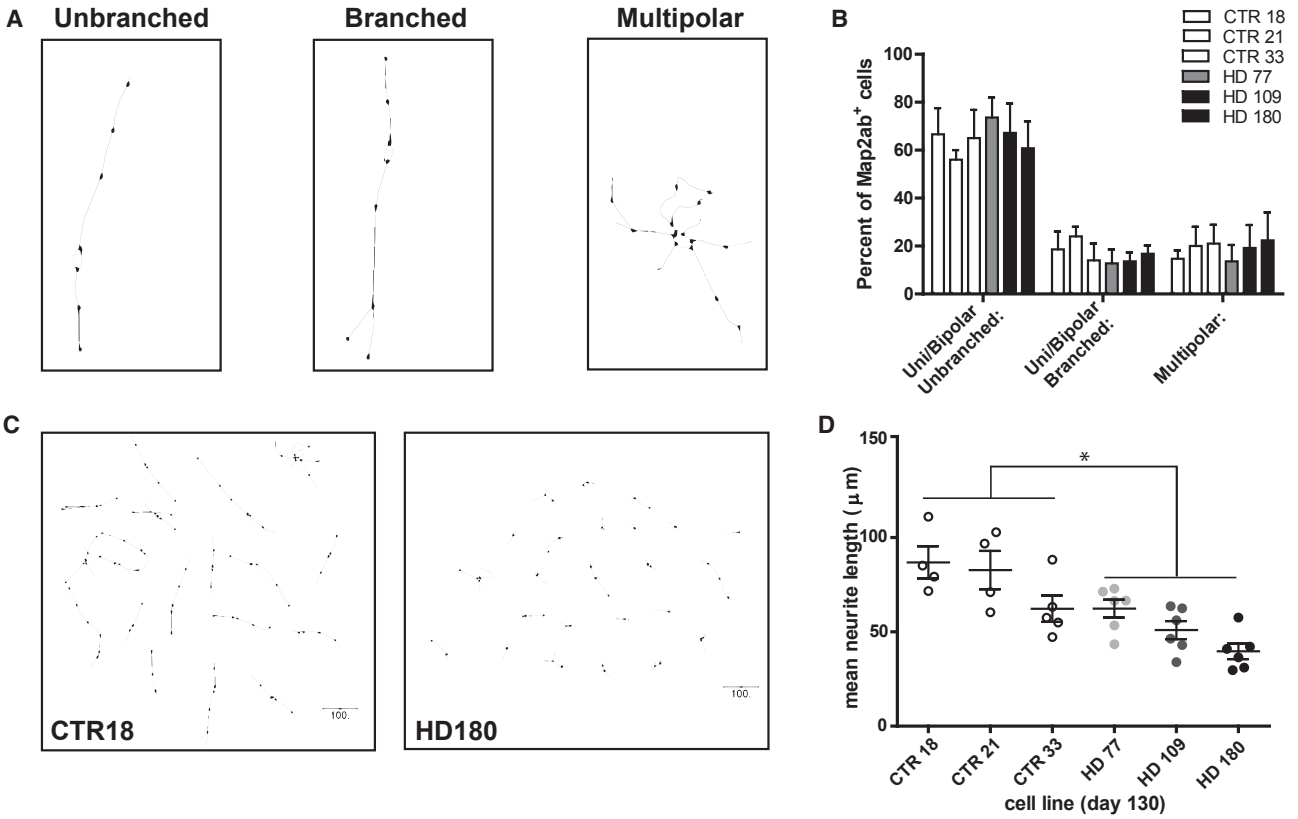

Figure 6. Transcriptomic Changes in the HD iPSC-Derived Cortical Cultures Manifest into Relevant Altered Morphological Phenotypes in Cortical Neurons

(A) Representative traces of the three morphologies of Map2ab+ iPSC-derived cortical neurons: unbranched, branched, and multipolar.

(B) Graphs of total percentage of Map2ab+ neurons at day 130 of differentiation displaying unbranched, branched, or multipolar morphology indicate there are no significant differences between populations of neurons displaying any one morphological type between HD and control.

(C) Representative traces of control (CTR18) and HD (HD180) iPSC-derived cortical Map2ab-positive neurons at 130 days of differentiation. Circles indicate the cell bodies and lines represent the individual neurites and their respective branching.

(D) HD iPSC-derived Map2ab+ cortical neurons at day 130 of differentiation had a CAG-length-dependent decrease in neurite length. The control samples had significantly longer neurite lengths than the HD samples (dotted line; $p = 0.0474$) with a strong correlation of CAG length and mean neurite length ($r = -0.7698$, $p < 0.0001$).

Data are presented as mean ± SEM. All cell counts were from at least three separate differentiations. Please see STAR Methods for statistical information.

neurite outgrowth measurements, HD samples showed a significant relationship between CAG-repeat expansion and altered phenotype. Of note, HD samples of varying CAG length showed a graded response, which has been previously demonstrated in the HD iPSC lines (HD iPSC Consortium, 2012). We also saw a graded response within the controls as well, as within the gene expression profiles (Figure 3), neurite length (Figure 6), and electrophysiology (Figure 7), the long-repeat control (CTR33) grouped between the other controls and HD lines. These results *in vitro* correlate with non-HD carriers, who show that increased repeats of Htt CAG within the non-pathogenic range correlate with greater overall changes in cortex structure (Lee et al., 2017). One thing yet to be investigated is whether the DEGs found in this study are representative of overall gene expression changes in all the cells within culture or whether they are reflective of large gene expression changes within a small subset of cells. This could be further uncovered with more advanced single-cell transcriptomic analysis.

Altered developmental signatures, followed by compensatory mechanisms for decades until formal disease onset, have been proposed for multiple adult-onset neurodegenerative diseases such as amytrophic lateral sclerosis (ALS) (van Zundert et al., 2012) and spinocerebellar ataxia 1 (Fujita et al., 2017) in addition to HD. Here, we demonstrate that the HD iPSC-derived cortical neurons also displayed a delayed electrophysiological maturation phenotype. This corroborates findings from iPSC-derived striatal cultures, which demonstrated developmental delays by transcriptomic analysis (HD iPSC Consortium, 2017) and reduced numbers of neural progenitor cells (Mattis et al., 2015). Although HD cortical neurons displayed reduced action potentials, both induced and spontaneous, at ~80 days of differentiation, by day 90+, they began to spontaneously fire, indicating that the HD neurons do mature with extended time. This correlates with overall DEGs at this time points, as the day 60–100 time points have the highest numbers of DEGs (222–568), but by day 130, the number of genes has dropped

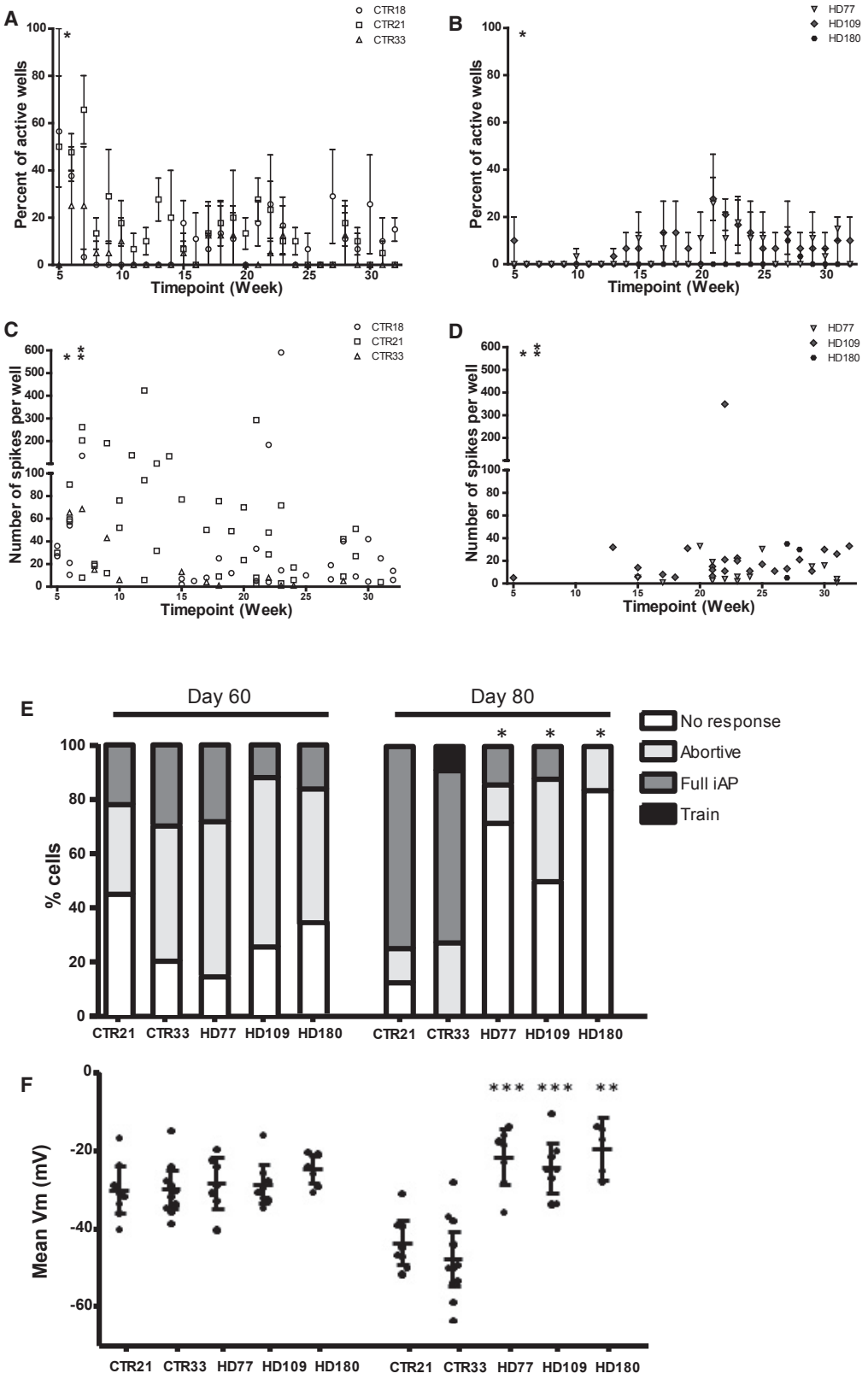

(legend on next page)

dramatically (55 DEGs). As it has been previously reported in murine models that mtHTT cannot compensate for the loss of wild-type Htt in order to establish cortical and striatal excitatory circuits (McKinstry et al., 2014), this delayed functional maturation phenotype may be indicative of overall circuitry dysfunction in human HD cortical neurons.

Murine models of HD have demonstrated that mtHTT expression alters the spindle orientation of dividing cortical progenitors (Molina-Calavita et al., 2014) and impairs mitosis. This reduces the overall thickness of the developing cortex (Molina-Calavita et al., 2014), with a greatly decreased layer VI thickness and an increased layer II–IV thickness (Molina-Calavita et al., 2014). Altered mitosis was clearly reflected in the GO term analysis of the HD cortical neuron DEGs (Table S3). However, examination of spindle orientation and cortical layer thickness is unreliable in 2D models, as they do not recapitulate the cortical lamination seen *in vivo* (Paşca et al., 2015). Therefore, using a 3D organoid model in the future will be essential to analyze potential cortical lamination phenotypes, because while these organoids do not form the exact cortical layering seen in the *in vivo* brain, they organize into recognizable deep and upper layers (Paşca et al., 2015; Lancaster et al., 2013; Qian et al., 2017; Sloan et al., 2017; Mariani et al., 2015). A recent publication using a 3D cerebral organoid model of HD demonstrated defects in developing cytoarchitecture and neuronal maturation (Conforti et al., 2018). These data were limited to the iPSC line but set the stage for future investigation. Therefore, in the future, 3D models of HD corticogenesis will provide much information regarding both potential altered development and functionality, as well as how dysfunctional neurodevelopment can later lead to neurodegeneration (Paşca et al., 2015).

The cortex does not function in a vacuum, and defects in the connectivity of the projection neurons of the cortex to those of the striatum have been well documented in HD murine models and patients (Gauthier et al., 2004; Zuccato et al., 2010; Cepeda et al., 2003; Gatto et al., 2015; Saudou and Humbert, 2016; Rosas et al., 2010; Tabrizi et al., 2011). Therefore, the next logical step in these experiments is to use 3D modeling to study the cortico-striatal function in HD iPSC-derived *in vitro* models. Previous studies have fused iPSC-derived organoids of cortical and medial ganglionic eminence regions, demonstrating functional interneuron migration into the cortex (Xiang et al., 2017). This paradigm could be easily adapted to use HD iPSC-derived cortical organoids fused to organoids of the lateral ganglionic eminence, from which the striatum arises, to examine the functionality of the cortico-striatal synapses. Alternately, microfluidic devices have been used to recapitulate the HD murine cortico-striatal network, demonstrating presynaptic defects that may be critical to the progression of HD (Virlogeux et al., 2018). Human iPSC-derived motor neurons and endothelial cells can be co-cultured on a microfluidic "organ-on-chip" platform in order to model cellular interactions involved in motor neuron diseases (Sances et al., 2018). HD iPSC-derived cortico-striatal networks grown on an organ-on-chip should advance the understanding of disease origin and progression, as well as drug development.

In conclusion, iPSCs generated from HD patients can be differentiated toward a cortical fate in a culture that generates neurons with transcriptomic, morphological, and functional phenotypes in a way that reflects an altered neurodevelopmental signature. In the future, this model can be used not only to further examine the role of mtHTT in human corticogenesis but also to find novel pathways for potential therapeutic intervention before onset of disease.

STAR★METHODS

Detailed methods are provided in the online version of this paper and include the following:

- KEY RESOURCES TABLE
- CONTACT FOR REAGENT AND RESOURCE SHARING
- EXPERIMENTAL MODEL AND SUBJECT DETAILS
- METHOD DETAILS
  - Cortical Differentiation from iPSCs
  - Immunocytochemistry and Cell Counting
  - Cellular Morphology Analysis
  - Electrophysiology
  - RNA extraction for RNA sequencing

Figure 7. iPSC-Derived Cortical Cultures Display Altered Induced and Spontaneous Electrophysiological Activity Potentially Reflective of a Delayed Functional Maturation Seen in Transcriptomic Analysis

(A) Multielectrode array (MEA) data demonstrate that the control cultures elicit spontaneous activity throughout the course of the experiment, as measured by the percentage of wells with active electrodes.

(B) MEA data demonstrate that there is a significant difference across groups and time ($p = 0.0049$). HD cultures only elicit spontaneous activity at a much later time point as compared to controls (A), as measured by the percentage of wells with active electrodes. There is a significant negative correlation across all times ($r_S = -0.244$, $p < 0.0001$), but stronger negative correlations are noted at earlier time points. There is also a significant CAG-length dependence of this phenotype ($p = 0.0103$). Asterisk (*) indicates an adjusted p value of 0.0021 in HD compared to controls of the single time point.

(C) Control cultures have spontaneous activity (as measured by spiking events over the course of 3 min) throughout the course of the experiment.

(D) HD cultures have spontaneous activity only at later stages. There is a significant difference across group and time ($p = 0.0054$) and a significant negative correlation across all times ($r_S = -0.261$, $p < 0.0001$), but stronger negative correlations are noted at earlier time points. Asterisks indicate an adjusted p value of 0.0017 (*) or 0.0038 (**) in HD compared to controls of the single time point.

(E) Proportions of cells in the cortical cultures at days 60 and 80 that are not able to elicit an induced action potential (iAP) (no response), abortive iAPs, full iAPs, or a train of iAPs. While similar in proportion between HD and control at day 60, by day 80, the HD cultures had significantly less maturation toward the more mature full or a train of iAPs seen in control cultures (*$p < 0.05$, HD compared to controls).

(F) While the control lines had a decreased resting membrane potential (RMP) from days 60 (left) to 80 (right), indicative of a more mature neuron, the HD cultures had a significantly similar or increased RMP in conjunction with the reduced ability to elicit a mature iAP (**$p < 0.01$, ***$p < 0.01$, HD lines as compared to controls of the same time point).

Data are presented as mean ± SEM. All electrophysiology was performed in at least two to three separate differentiations. Please see STAR Methods for statistical information.

SUPPLEMENTAL INFORMATION

Supplemental Information includes five figures and three tables and can be found with this article online at https://doi.org/10.1016/j.celrep.2018.09.076.

ACKNOWLEDGMENTS

The authors would like to thank Dr. Soshana Svendsen for critical review and editing of the manuscript, Drs. Clive Svendsen and Ritchie Ho for helpful insight, Michael Workman for assistance with the WGCNA, and Dr. Veronica Garcia for training on the MEA system. We would also like to thank the Cedars-Sinai iPSC Core Facility for generating the HD and non-diseased iPSCs and the Genomics Core for the RNA sequencing and analysis. This work was supported by The Board of Governors Regenerative Medicine Institute and by Cedars-Sinai in support of CTSI grant UL1TR001881-01.

AUTHOR CONTRIBUTIONS

S.R.M., C.M.T., D.R., and V.B.M. performed the experiments. Y.W., J.T., V.B.M., and P.P.M. performed transcriptomic data analyses. C.B., Y.W., and D.R. performed statistical analysis. V.B.M. designed the experiments and wrote the manuscript.

DECLARATION OF INTERESTS

The authors declare no competing interests.

Received: March 27, 2018
Revised: September 2, 2018
Accepted: September 24, 2018
Published: October 23, 2018

SUPPORTING CITATIONS

The following reference appears in the Supplemental Information: Heberle et al. (2015).

REFERENCES

An, M.C., Zhang, N., Scott, G., Montoro, D., Wittkop, T., Mooney, S., Melov, S., and Ellerby, L.M. (2012). Genetic correction of Huntington's disease phenotypes in induced pluripotent stem cells. Cell Stem Cell *11*, 253–263.

Andrew, S.E., Goldberg, Y.P., Kremer, B., Telenius, H., Theilmann, J., Adam, S., Starr, E., Squitieri, F., Lin, B., Kalchman, M.A., et al. (1993). The relationship between trinucleotide (CAG) repeat length and clinical features of Huntington's disease. Nat. Genet. *4*, 398–403.

Barnat, M., Le Friec, J., Benstaali, C., and Humbert, S. (2017). Huntingtin-mediated multipolar-bipolar transition of newborn cortical neurons is critical for their postnatal neuronal morphology. Neuron *93*, 99–114.

Cepeda, C., Hurst, R.S., Calvert, C.R., Hernández-Echeagaray, E., Nguyen, O.K., Jocoy, E., Christian, L.J., Ariano, M.A., and Levine, M.S. (2003). Transient and progressive electrophysiological alterations in the corticostriatal pathway in a mouse model of Huntington's disease. J. Neurosci. *23*, 961–969.

Clowry, G., Molnár, Z., and Rakic, P. (2010). Renewed focus on the developing human neocortex. J. Anat. *217*, 276–288.

Conforti, P., Besusso, D., Bocchi, V.D., Faedo, A., Cesana, E., Rossetti, G., Ranzani, V., Svendsen, C.N., Thompson, L.M., Toselli, M., et al. (2018). Faulty neuronal determination and cell polarization are reverted by modulating HD early phenotypes. Proc. Natl. Acad. Sci. USA *115*, E762–E771.

Cummings, D.M., Cepeda, C., and Levine, M.S. (2010). Alterations in striatal synaptic transmission are consistent across genetic mouse models of Huntington's disease. ASN Neuro *2*, e00036.

Cummings, D.M., Milnerwood, A.J., Dallérac, G.M., Waights, V., Brown, J.Y., Vatsavayai, S.C., Hirst, M.C., and Murphy, K.P. (2006). Aberrant cortical synaptic plasticity and dopaminergic dysfunction in a mouse model of Huntington's disease. Hum. Mol. Genet *15*, 2856–2868.

Cummings, D.M., Milnerwood, A.J., Dellérac, G.M., Vatsavayai, S.C., Hirst, M.C., and Murphy, K.P. (2007). Abnormal cortical synaptic plasticity in a mouse model of Huntington's disease. Brain Res. Bull *72*, 103–107.

Dobin, A., Davis, C.A., Schlesinger, F., Drenkow, J., Zaleski, C., Jha, S., Batut, P., Chaisson, M., and Gingeras, T.R. (2013). STAR: ultrafast universal RNA-seq aligner. Bioinformatics *29*, 15–21.

Dolmetsch, R., and Geschwind, D.H. (2011). The human brain in a dish: the promise of iPSC-derived neurons. Cell *145*, 831–834.

Duyao, M., Ambrose, C., Myers, R., Novelletto, A., Persichetti, F., Frontalia, M., Folstein, S., Ross, C., Franz, M., Abbott, M., et al. (1993). Trinucleotide repeat length instability and age of onset in Huntington's disease. Nat. Genet *4*, 387–392.

Fennema-Notestine, C., Archibald, S.L., Jacobson, M.W., Corey-Bloom, J., Paulsen, J.S., Peavy, G.M., Gamst, A.C., Hamilton, J.M., Salmon, D.P., and Jernigan, T.L. (2004). *In vivo* evidence of cerebellar atrophy and cerebral white matter loss in Huntington disease. Neurology *63*, 989–995.

Fujita, K., Mao, Y., Uchida, S., Chen, X., Shiwaku, H., Tamura, T., Ito, H., Watase, K., Homma, H., Tagawa, K., et al. (2017). Developmental YAPdeltaC determines adult pathology in a model of spinocerebellar ataxia type 1. Nat. Commun. *8*, 1864.

Gatto, R.G., Chu, Y., Ye, A.Q., Price, S.D., Tavassoli, E., Buenaventura, A., Brady, S.T., Magin, R.L., Kordower, J.H., and Morfini, G.A. (2015). Analysis of YFP(J16)-R6/2 reporter mice and postmortem brains reveals early pathology and increased vulnerability of callosal axons in Huntington's disease. Hum. Mol. Genet. *24*, 5285–5298.

Gauthier, L.R., Charrin, B.C., Borrell-Pagès, M., Dompierre, J.P., Rangone, H., Cordelières, F.P., De Mey, J., MacDonald, M.E., Lessmann, V., Humbert, S., and Saudou, F. (2004). Huntingtin controls neurotrophic support and survival of neurons by enhancing BDNF vesicular transport along microtubules. Cell *118*, 127–138.

Gauthier-Fisher, A., Lin, D.C., Greeve, M., Kaplan, D.R., Rottapel, R., and Miller, F.D. (2009). Lfc and Tctex-1 regulate the genesis of neurons from cortical precursor cells. Nat. Neurosci. *12*, 735–744.

Godin, J.D., Colombo, K., Molina-Calavita, M., Keryer, G., Zala, D., Charrin, B.C., Dietrich, P., Volvert, M.L., Guillemot, F., Dragatsis, I., et al. (2010). Huntingtin is required for mitotic spindle orientation and mammalian neurogenesis. Neuron *67*, 392–406.

Handel, A.E., Chintawar, S., Lalic, T., Whiteley, E., Vowles, J., Giustacchini, A., Argoud, K., Sopp, P., Nakanishi, M., Bowden, R., et al. (2016). Assessing similarity to primary tissue and cortical layer identity in induced pluripotent stem cell-derived cortical neurons through single-cell transcriptomics. Hum. Mol. Genet. *25*, 989–1000.

HDCRG (Huntington's Disease Collaborative Research Group) (1993). A novel gene containing a trinucleotide repeat that is expanded and unstable on Huntington's disease chromosomes. Cell *72*, 971–983.

HD iPSC Consortium (2012). Induced pluripotent stem cells from patients with Huntington's disease show CAG-repeat-expansion-associated phenotypes. Cell Stem Cell *11*, 264–278.

HD iPSC Consortium (2017). Developmental alterations in Huntington's disease neural cells and pharmacological rescue in cells and mice. Nat. Neurosci *20*, 648–660.

Heberle, H., Meirelles, G.V., da Silva, F.R., Telles, G.P., and Minghim, R. (2015). InteractiVenn: a web-based tool for the analysis of sets through Venn diagrams. BMC Bioinformatics *16*, 169.

Hickey, M.A., and Chesselet, M.F. (2003). Apoptosis in Huntington's disease. Prog. Neuropsychopharmacol. Biol. Psychiatry *27*, 255–265.

Hodges, A., Strand, A.D., Aragaki, A.K., Kuhn, A., Sengstag, T., Hughes, G., Elliston, L.A., Hartog, C., Goldstein, D.R., Thu, D., et al. (2006). Regional and cellular gene expression changes in human Huntington's disease brain. Hum. Mol. Genet. *15*, 965–977.

Huang, D.W., Sherman, B.T., Tan, Q., Collins, J.R., Alvord, W.G., Roayaei, J., Stephens, R., Baseler, M.W., Lane, H.C., and Lempicki, R.A. (2007a). The DAVID Gene Functional Classification Tool: a novel biological module-centric algorithm to functionally analyze large gene lists. Genome Biol. *8*, R183.

Huang, D.W., Sherman, B.T., Tan, Q., Kir, J., Liu, D., Bryant, D., Guo, Y., Stephens, R., Baseler, M.W., Lane, H.C., and Lempicki, R.A. (2007b). DAVID Bioinformatics Resources: expanded annotation database and novel algorithms to better extract biology from large gene lists. Nucleic Acids Res. *35*, W169–W175.

Lancaster, M.A., Renner, M., Martin, C.A., Wenzel, D., Bicknell, L.S., Hurles, M.E., Homfray, T., Penninger, J.M., Jackson, A.P., and Knoblich, J.A. (2013). Cerebral organoids model human brain development and microcephaly. Nature *501*, 373–379.

Langfelder, P., and Horvath, S. (2008). WGCNA: an R package for weighted correlation network analysis. BMC Bioinformatics *9*, 559.

Lee, J.K., Mathews, K., Schlaggar, B., Perlmutter, J., Paulsen, J.S., Epping, E., Burmeister, L., and Nopoulos, P. (2012). Measures of growth in children at risk for Huntington disease. Neurology *79*, 668–674.

Lee, J.K., Ding, Y., Conrad, A.L., Cattaneo, E., Epping, E., Mathews, K., Gonzalez-Alegre, P., Cahill, L., Magnotta, V., Schlaggar, B.L., et al. (2017). Sex-specific effects of the Huntington gene on normal neurodevelopment. J. Neurosci. Res. *95*, 398–408.

Li, B., and Dewey, C.N. (2011). RSEM: accurate transcript quantification from RNA-Seq data with or without a reference genome. BMC Bioinformatics *12*, 323.

Macdonald, V., and Halliday, G. (2002). Pyramidal cell loss in motor cortices in Huntington's disease. Neurobiol. Dis. *10*, 378–386.

Magnuson, T., Epstein, C.J., Silver, L.M., and Martin, G.R. (1982). Pluripotent embryonic stem cell lines can be derived from tw5/tw5 blastocysts. Nature *298*, 750–753.

Mariani, J., Coppola, G., Zhang, P., Abyzov, A., Provini, L., Tomasini, L., Amenduni, M., Szekely, A., Palejev, D., Wilson, M., et al. (2015). FOXG1-dependent dysregulation of GABA/glutamate neuron differentiation in autism spectrum disorders. Cell *162*, 375–390.

Marzesco, A.M., Mora-Bermudez, F., and Huttner, W.B. (2009). Neurogenesis in G minor. Nat. Neurosci. *12*, 669–671.

Mattis, V.B., and Svendsen, C.N. (2017). Modeling Huntington's disease with patient-derived neurons. Brain Res. *1656*, 76–87.

Mattis, V.B., Tom, C., Akimov, S., Saeedian, J., Østergaard, M.E., Southwell, A.L., Doty, C.N., Ornelas, L., Sahabian, A., Lenaeus, L., et al. (2015). HD iPSC-derived neural progenitors accumulate in culture and are susceptible to BDNF withdrawal due to glutamate toxicity. Hum. Mol. Genet. *24*, 3257–3271.

McKinstry, S.U., Karadeniz, Y.B., Worthington, A.K., Hayrapetyan, V.Y., Ozlu, M.I., Serafin-Molina, K., Risher, W.C., Ustunkaya, T., Dragatsis, I., Zeitlin, S., et al. (2014). Huntingtin is required for normal excitatory synapse development in cortical and striatal circuits. J. Neurosci. *34*, 9455–9472.

Molero, A.E., Gokhan, S., Gonzalez, S., Feig, J.L., Alexandre, L.C., and Mehler, M.F. (2009). Impairment of developmental stem cell-mediated striatal neurogenesis and pluripotency genes in a knock-in model of Huntington's disease. Proc. Natl. Acad. Sci. USA *106*, 21900–21905.

Molero, A.E., Arteaga-Bracho, E.E., Chen, C.H., Gulinello, M., Winchester, M.L., Pichamoorthy, N., Gokhan, S., Khodakhah, K., and Mehler, M.F. (2016). Selective expression of mutant huntingtin during development recapitulates characteristic features of Huntington's disease. Proc. Natl. Acad. Sci. USA *113*, 5736–5741.

Molina-Calavita, M., Barnat, M., Elias, S., Aparicio, E., Piel, M., and Humbert, S. (2014). Mutant huntingtin affects cortical progenitor cell division and development of the mouse neocortex. J. Neurosci. *34*, 10034–10040.

Neueder, A., and Bates, G.P. (2014). A common gene expression signature in Huntington's disease patient brain regions. BMC Med. Genomics *7*, 60.

Nopoulos, P.C., Aylward, E.H., Ross, C.A., Johnson, H.J., Magnotta, V.A., Juhl, A.R., Pierson, R.K., Mills, J., Langbehn, D.R., and Paulsen, J.S.; PREDICT-HD Investigators Coordinators of Huntington Study Group (HSG) (2010). Cerebral cortex structure in prodromal Huntington disease. Neurobiol. Dis. *40*, 544–554.

O'Kusky, J.R., Nasir, J., Cicchetti, F., Parent, A., and Hayden, M.R. (1999). Neuronal degeneration in the basal ganglia and loss of pallido-subthalamic synpases in mice with targeted disruption of the Huntington's disease gene. Brain Res *818*, 468–479.

Oyama, F., Miyazaki, H., Sakamoto, N., Becquet, C., Machida, Y., Kaneko, K., Uchikawa, C., Suzuki, T., Kurosawa, M., Ikeda, T., et al. (2006). Sodium channel beta4 subunit: down-regulation and possible involvement in neuritic degeneration in Huntington's disease transgenic mice. J. Neurochem. *98*, 518–529.

Paşca, A.M., Sloan, S.A., Clarke, L.E., Tian, Y., Makinson, C.D., Huber, N., Kim, C.H., Park, J.Y., O'Rourke, N.A., Nguyen, K.D., et al. (2015). Functional cortical neurons and astrocytes from human pluripotent stem cells in 3D culture. Nat. Methods *12*, 671–678.

Patino, G.A., and Isom, L.L. (2010). Electrophysiology and beyond: multiple roles of Na+ channel β subunits in development and disease. Neurosci. Lett. *486*, 53–59.

Qian, X., Nguyen, H.N., Jacob, F., Song, H., and Ming, G.L. (2017). Using brain organoids to understand Zika virus-induced microcephaly. Development *144*, 952–957.

Reiner, A., Del Mar, N., Meade, C.A., Yang, H., Dragatsis, I., Zeitlin, S., and Goldowitz, D. (2001). Neurons lacking huntingtin differentially colonize brain and survive in chimeric mice. J. Neurosci *21*, 7608–7619.

Reis, S.A., Thompson, M.N., Lee, J.M., Fossale, E., Kim, H.H., Liao, J.K., Moskowitz, M.A., Shaw, S.Y., Dong, L., Haggarty, S.J., et al. (2011). Striatal neurons expressing full-length mutant huntingtin exhibit decreased N-cadherin and altered neuritogenesis. Hum. Mol. Genet. *20*, 2344–2355.

Rosas, H.D., Lee, S.Y., Bender, A.C., Zaleta, A.K., Vangel, M., Yu, P., Fischl, B., Pappu, V., Onorato, C., Cha, J.H., et al. (2010). Altered white matter microstructure in the corpus callosum in Huntington's disease: implications for cortical "disconnection". Neuroimage *49*, 2995–3004.

Sances, S., Ho, R., Vatine, G., West, D., Laperle, A., Meyer, A., Godoy, M., Kay, P.S., Mandefro, B., Hatada, S., hinjosa, C., Wen, N., Sareen, D., Hamilton, G.A., and Svendsen, C.N. (2018). Human iPSC-derived endothelial cells microengineered organ-chip enhance neuronal development. Stem Cell Reports *10*, 1222–1236.

Saudou, F., and Humbert, S. (2016). The biology of Huntingtin. Neuron *89*, 910–926.

Shi, Y., Kirwan, P., and Livesey, F.J. (2012). Directed differentiation of human pluripotent stem cells to cerebral cortex neurons and neural networks. Nat. Protoc. *7*, 1836–1846.

Sloan, S.A., Darmanis, S., Huber, N., Khan, T.A., Birey, F., Caneda, C., Reimer, R., Quake, S.R., Barres, B.A., and Paşca, S.P. (2017). Human astrocyte maturation captured in 3D cerebral cortical spheroids derived from pluripotent stem cells. Neuron *95*, 779–790.e6.

Stern, E.A. (2011). Functional changes in neocortical activity in Huntington's disease model mice: an in vivo intracellular study. Front. Syst. Neurosci. *5*, 47.

Tabrizi, S.J., Scahill, R.I., Durr, A., Roos, R.A., Leavitt, B.R., Jones, R., Landwehrmeyer, G.B., Fox, N.C., Johnson, H., Hicks, S.L., et al.; TRACK-HD Investigators (2011). Biological and clinical changes in premanifest and early stage Huntington's disease in the TRACK-HD study: the 12-month longitudinal analysis. Lancet Neurol. *10*, 31–42.

Takahashi, K., and Yamanaka, S. (2006). Induction of pluripotent stem cells from mouse embryonic and adult fibroblast cultures by defined factors. Cell *126*, 663–676.

Thu, D.C., Oorschot, D.E., Tippett, L.J., Nana, A.L., Hogg, V.M., Synek, B.J., Luthi-Carter, R., Waldvogel, H.J., and Faull, R.L. (2010). Cell loss in the motor

and cingulate cortex correlates with symptomatology in Huntington's disease. Brain *133*, 1094–1110.

Tong, Y., Ha, T.J., Liu, L., Nishimoto, A., Reiner, A., and Goldowitz, D. (2011). Spatial and temporal requirements for huntingtin (Htt) in neuronal migration and survival during brain development. J. Neurosci. *31*, 14794–14799.

Unschuld, P.G., Joel, S.E., Liu, X., Shanahan, M., Margolis, R.L., Biglan, K.M., Bassett, S.S., Schretlen, D.J., Redgrave, G.W., van Zijl, P.C., et al. (2012). Impaired cortico-striatal functional connectivity in prodromal Huntington's Disease. Neurosci. Lett. *514*, 204–209.

van Zundert, B., Izaurieta, P., Fritz, E., and Alvarez, F.J. (2012). Early pathogenesis in the adult-onset neurodegenerative disease amyotrophic lateral sclerosis. J. Cell. Biochem. *113*, 3301–3312.

Virlogeux, A., Moutaux, E., Christaller, W., Genoux, A., Bruyère, J., Fino, E., Charlot, B., Cazorla, M., and Saudou, F. (2018). Reconstituting corticostriatal network on-a-chip reveals the contribution of the presynaptic compartment to Huntington's disease. Cell Rep. *22*, 110–122.

Vonsattel, J.P., Keller, C., and Del Pilar Amaya, M. (2008). Neuropathology of Huntington's disease. Handb. Clin. Neurol. *89*, 599–618.

White, J.K., Auerbach, W., Duyao, M.P., Vonsattel, J.P., Gusella, J.F., Joyner, A.L., and MacDonald, M.E. (1997). Huntingtin is required for neurogenesis and is not impaired by the Huntington's disease CAG expansion. Nat. Genet *17*, 404–410.

Xiang, Y., Tanaka, Y., Patterson, B., Kang, Y.J., Govindaiah, G., Roselaar, N., Cakir, B., Kim, K.Y., Lombroso, A.P., Hwang, S.M., et al. (2017). Fusion of regionally specified hPSC-derived organoids models human brain development and interneuron migration. Cell Stem Cell *21*, 383–398.e7.

Zhang, B., and Horvath, S. (2005). A general framework for weighted gene co-expression network analysis. Stat. Appl. Genet. Mol. Biol *4*, Article 17.

Zuccato, C., Valenza, M., and Cattaneo, E. (2010). Molecular mechanisms and potential therapeutical targets in Huntington's disease. Physiol. Rev. *90*, 905–981.

STAR★METHODS

KEY RESOURCES TABLE

REAGENT or RESOURCE	SOURCE	IDENTIFIER
Antibodies		
Ki67	Vector Laboratories	Cat# VP-K451, RRID:AB_2314701
Nestin	Abcam	Cat# ABD69, RRID:AB_2744681
SSEA4	Stemgent	Cat# EB09006, RRID:AB_2179791
FOXG1	Abcam	Cat# ab18259, RRID:AB_732415
ZO1	Invitrogen	Cat# 61-7300, RRID:AB_138452
DCX	Aves labs	Cat# DCX, RRID:AB_2313540
Beta-Tubulin III/TUJ1	Sigma-Aldrich	Cat# T8660, RRID:AB_477590
Map2ab	Sigma	Cat# M1406, RRID:AB_477171
TBR2	Abcam	Cat# ab23345, RRID:AB_778267
TBR1	Abcam	Cat# ab31940, RRID:AB_2200219
Ctip2	Abcam	Cat# ab18465, RRID:AB_2064130
SatB2	Abcam	Cat# ab51502, RRID:AB_882455
GFAP	Aves labs	Cat# LS-C51002-100, RRID:AB_1220403
Donkey anti-Mouse IgG (H+L) Highly Cross-Adsorbed, Alexa Fluor® 488	Life Technologies	Cat# A-21202, RRID:AB_141607
Donkey anti-Mouse IgG (H+L) Highly Cross-Adsorbed, Alexa Fluor® 647	Life Technologies	Cat# A-31571, RRID:AB_162542
Goat anti-Mouse IgG (H+L) Cross-Adsorbed, Alexa Fluor® 594	Life Technologies	Cat# A-11005, RRID:AB_141372
Donkey anti-Rabbit IgG (H+L) Highly Cross-Adsorbed, Alexa Fluor® 488	Life Technologies	Cat# A-21206, RRID:AB_141708
Donkey anti-Rabbit IgG (H+L) Highly Cross-Adsorbed, Alexa Fluor® 594	Life Technologies	Cat# A-21207, RRID:AB_141637
Donkey anti-Rabbit IgG (H+L) Highly Cross-Adsorbed, Alexa Fluor® 647	Life Technologies	Cat# A-31573, RRID:AB_2536183
Chemicals, Peptides, and Recombinant Proteins		
Matrigel	Corning	354230
mTeSR	StemCell Technologies, Inc.	5850
EZ tool	Life Technologies	23181-010
rock inhibitor (Y27632)	Tocris	1254
DMEM:F12	Life Technologies	11330
Neurobasal	Life Technologies	21103-049
Insulin	Sigma-Aldrich	I9278-5ML
NEAA	Life Technologies	11140-050
L-Glutamine	Life Technologies	25030-081
antibiotic/antimycotic	Life Technologies	15240-062
N2	Life Technologies	17502048
B27	Life Technologies	17504044
SB43142	Tocris	1614
LDN193189	Selleck	S2618
TrypLE	Thermofisher	12604013
FGF2	Peprotech	100-18B
paraformaldehyde	EMS	1224SK-SP

(*Continued on next page*)

Continued

REAGENT or RESOURCE	SOURCE	IDENTIFIER
4′,6-diamidino-2-phenylindole (DAPI)	molecular probes	D3571
1mm OD thin wall glass capillaries	Fisher Scientific	22-362566
Trizol	Thermo Fischer Scientific	155596026
choloroform	Sigma-Aldrich	C2432-25ML
RNeasy column	QIAGEN	74106
RNase-free DNase	QIAGEN	79254
reverse transcriptase	Invitrogen	LS18064022
Agencourt AMPure XP beads	Beckman Coulter	A63880
Critical Commercial Assays		
48 well microarray electrode array (MEA) plates	Axion Biosystems	M768-KAP-48
96 well microarray electrode array (MEA) plates	Axion Biosystems	M768-KAP-96
TruSeq Stranded mRNA library preparation kit	Illumina	20020594
Deposited Data		
Raw data and statistical analysis (Mendeley Data)	This paper	https://doi.org/10.17632/y275mydz78.1
RNA sequencing data	This paper	GEO: GSE109534
Experimental Models: Cell Lines		
CS97iHD180n; male, 6 years	iPSC Core (CSMC)	CS97iHD180n
CS09iHD109n; female, age unknown	iPSC Core (CSMC)	CS09iHD109n
CS77iHD77n; male, age unknown	iPSC Core (CSMC)	CS77iHD77n
CS83iCTR33n; female, 21 years	iPSC Core (CSMC)	CS83iCTR33n
CS00iCTR21n; male, 6 years	iPSC Core (CSMC)	CS00iCTR21n
CS25iCTR18n; male, 76 years	iPSC Core (CSMC)	CS25iCTR18n
Experimental Models: Organisms/Strains		
Qubit fluorometer	ThermoFisher Scientific	Qubit fluorometer
2100 Bioanalyzer	Agilent Technologies	2100 Bioanalyzer
Software and Algorithms		
Neuroleucida 11.07.3	MBF Biosciences	v11.07.3
Neuroexplorer 360 11.09	MBF Biosciences	v11.09
Maestro Axis software version 2.4.2	Axion Biosystems	v2.4.2
Plexon Offline Sorter, v4.3.1	Plexon	v4.3.1
STAR (version 2.5.0) / RSEM (version 1.2.25)	http://code.google.com/p/rna-star/	Open source
DESeq2 Bioconductor package version 1.10.1 in R version 3.2.2	https://bioconductor.org/packages/release/bioc/html/DESeq2.html	Open source
Bioconductor g-plots package (version 2.14.2) in R	https://www.bioconductor.org/install/	Open source
DAVID Bioinformatics database (version 6.8)	https://david.ncifcrf.gov/	Open source
WGCNA was performed using its package in R	https://cran.r-project.org/web/packages/WGCNA/index.html	Open source
SAS v9.4 software	SAS Institute Inc.	v9.4

CONTACT FOR REAGENT AND RESOURCE SHARING

Further information and requests for resources and reagents should be directed to and will be fulfilled by the Lead Contact, Virginia Mattis (virginiamattis@gmail.com). Requests for iPSC lines can be made to the CSMC Board of Governors Regenerative Medicine Institute iPSC Core and will require an MTA.

EXPERIMENTAL MODEL AND SUBJECT DETAILS

Human fibroblast lines were obtained from three HD patients with a CAG-expanded HTT allele with 180 (CS97iHD180n; male, 6 years), 109 (CS09iHD109n; female, age unknown), or 77 repeats (CS77iHD77n; male, age unknown), and from three non-HD

"controls" with 33 (CS83iCTR33n; female, 21 years), 21 (CS00iCTR21n; male, 6 years), or 18 (CS25iCTR18n; male, 76 years) repeat CAG alleles. These lines were all approved for use under IRB/SCRO protocols Pro00021505 and Pro00024899.

METHOD DETAILS

Cortical Differentiation from iPSCs

Reprogramming was conducted by non-integrating methods, as previously described (Mattis et al., 2015; HD iPSC Consortium, 2017). These iPSC lines were fully reprogrammed as demonstrated by staining for alkaline phosphatase and other pluripotency makers, passed the 'PluriTest' assessed by characterization of low 'novelty' and high 'pluripotency' gene expression and grouped away from the original fibroblast source (Mattis et al., 2015). Southern blotting and genomic polymerase chain reaction (PCR) analyses confirmed the absence of plasmid gene expression after several passages, confirming that there was no integration of the reprogramming plasmids (Mattis et al., 2015). The iPSCs were also easy to grow, remained karyotypically normal over many passages and could be efficiently banked to provide resources for future experiments and collaborators. CAG length was analyzed and, as we have previously reported (HD iPSC Consortium, 2012), while no expansion was seen within the control lines, some expansion was seen in the HD iPSC lines (data not shown).

iPSCs were differentiated toward a cortical fate as described in Shi et al. (Shi et al., 2012), with some modifications as described here. iPSCs were grown on Matrigel (Corning 354230) in mTeSR (StemCell Technologies, Inc. 5850) at 37 degrees and with 5% O_2 until they reached 70% confluency. They were then passaged with an EZ tool (Life Technologies 23181-010) and plated in a 2:1 ratio with rock inhibitor (10 μM Y27632, Tocris 1254) in mTeSR on matrigel. When the cells reached 100% confluency they were switched to cortical NIM (1:1 DMEM:F12 (Life Technologies 11330): Neurobasal (Life Technologies 21103-049), 2.5 μg/ml Insulin (Sigma-Aldrich I9278-5ML), 0.5% NEAA (Life Technologies 11140-050), 0.5% L-Glutamine (Life Technologies 25030-081), 1% antibiotic/antimycotic (Life Technologies 15240-062), 0.5% N2 (Life Technologies 17502048), 1% B27 (Life Technologies 17504044), 10 μM SB43142 (Tocris 1614), 2 μM LDN193189 (Selleck S2618)) with daily media changes. They were passaged at day 12 with TrypLE (Thermofisher 12604013) and replated at a 1:2 ratio. The next day they were refed with cortical NMM (1:1 DMEM:F12: Neurobasal, 2.5 μg/ml Insulin, 0.5% NEAA, 0.5% L-Glutamine, 1% antibiotic/antimycotic, 0.5% N2, 1% B27) with 20ng/ml FGF2 (Peprotech 100-18B) for the next four days, after which FGF2 was removed from the media. Cells were passaged using TrypLE and expanded 1:2 as necessary after this point until day 32. At day 32-35 cells were single-cell dissociated using TrypLE (5 min at 37°C), washed in DMEM and resuspended in NMM to plate onto PLO-treated and Matrigel-coated coverslips at 100,000 cells per coverslip. Cells were grown in NMM until time points described in the text. Half-media changes were performed every 2-3 days, as needed.

Immunocytochemistry and Cell Counting

All cells were plated and differentiated on poly-lysine and matrigel-coated coverslips before being fixed in 3.2% paraformaldehyde (EMS 1224SK-SP) at time points indicated in the text. After fixation, cells were rinsed with phosphate buffered saline (PBS; Corning 21-030-CV) and permeabilized using 0.2% Triton X-100 in PBS for 10 min at room temperature. Cells were then labeled with primary antibodies Ki67 (VP-K451; 1:1000), Nestin (Abcam ABD69; 1:10,000), SSEA4 (Stemgent 09-006; 1:100), FOXG1 (Abcam ab18259; 1:300), DCX (Aves labs DCX; 1:200), ZO1 (Invitrogen 617300; 1:100), Beta-Tubulin III/TUJ1 (Sigma-Aldrich T8660, 1:1000), Map2ab (Sigma m1408; 1:250), TBR2 (Abcam ab23345; 1:200), TBR1 (Abcam ab31940; 1:300), Ctip2 (Abcam ab18465; 1:300), SatB2 (Abcam ab51502; 1:100), and/or GFAP (Aves labs GFAP; 1:250) for 60 min at room temperature or overnight at 4°C. Coverslips were then exposed to the appropriate fluorescently tagged secondary antibodies for 60 min at room temperature (Alexa Fluor 488, 594 or 647 1:500 (Life Technologies A-21202, A-31571, A-11005, A-21206, A-21207, A-31573)). 4′,6-diamidino-2-phenylindole (DAPI; molecular probes D3571) was used to label nuclei. All experiments were performed on at least three separate differentiations. All immunochemistry was visualized on a Leica microscope using a 20 × objective.

Non-biased stereological quantification was performed using the optical fractionator method (MBF Biosciences, Williston, Vermont, USA) paired with a Zeiss microscope in order quantify the total percentage of cells (DAPI-expressing nuclei) expressing a given marker. Each coverslip was individually traced and cells were counted with a 20x objective, using a counting frame size of 20 × 20 μm and a 1000 × 1000 μm distance between the counting frames. At least one coverslip was analyzed at each time point for each cell line for each cell marker from at least three separate experimental differentiations.

Cellular Morphology Analysis

$Map2ab^+$ neurons were randomly selected from blinded slides and live traced using Neuroleucida 11.07.3 (MicroBrightField, VT, USA) on a Axio Imager 2 (Zeiss, Oberkochen, Germany) microscope at 20x magnification. Neuronal mapping was done first by contouring the cell soma and then the connected neurites, by tracing a graph of points through the midlines of the Map2ab extensions. A single cell soma with all its dendrites was classified as one dataset, twenty-five datasets were recorded for each blinded coverslip. Neuronal reconstruction and visualization was accomplished using the companion software module, Neuroexplorer 360 11.09. Each neuron was classified based on dendritic morphology (Branched/ Unbranched/ Multipolar) and multiple branch structure analyses were carried out such as length of each dendritic segment, number of segments of each branching order, number of nodes, dimensions of soma and neuronal processes. The mean percentage of each dendritic morphology (Branched/ Unbranched/ Multipolar) as well as average dendritic length of each individual differentiation was calculated, which was then used to establish the mean dendritic

length and morphology across a particular cell line. At least 50 neurite lengths were measured per experiment, with at least three independent experimental repeats.

Electrophysiology

Patch Clamp: Glass micropipettes were pulled using a Sutter Instruments P-1000 from WPI 1mm OD thin wall glass capillaries (Fisher Scientific 22-362566) with a tip resistance of between 4 and 6 MΩ. Whole cell patch clamp was performed on a Leica DM-LED microscope on an air table, using Scientifica Patchstar manipulators. Voltage and current clamp recordings were performed using a Molecular Devices Multiclamp 700b amplifier, Digidata 1300 digital to and from analog converter, and Pclamp 10 acquisition software. Cells were bathed in an extracellular solution (ECS) containing 135mM NaCl, 5mM KCl, 5mM HEPES, 10mM Glucose, 1.2mM $MgCl_2$ and 1.25mM $CaCl_2$. The internal solution contained 10mM NaCl, 117mM KCl, 11mM HEPES, 2mM Na.ATP, 2mM $MgCl_2$ and 1mM $CaCl_2$. In current clamp, the cell's resting membrane voltage was assessed by averaging from continuous voltage recordings while holding the current at 0pA. Induced action potentials were recorded in fast current clamp mode during a current step protocol; current was injected to hold the membrane potential at ca. −70 mV and then 100 ms current injection was applied, starting with 0 pA and increasing to 180 pA in 10 pA increments in each successive sweep.

Multi-Electrode Array (MEA): MEA experiments were performed in two to three experimental repeats, with at least three wells assayed per experiment. 47,500 cells were plated per cm^2 in either 48 (Axion Biosystems M768-KAP-48) or 96 (Axion Biosystems M768-KAP-96) well microarray electrode array (MEA) plates at approximately 35 days of differentiation. MEA data was recorded using the Maestro MEA system (Axion Biosystems). The recording sampling frequency was set to 12.5kHz and the analog settings were set to standard neural spikes (1200X Gain, 2000 – 5000 Hz, Axion Biosystems Maestro Axis software version 2.4.2). A Butterworth band pass filter was applied, with the high and low pass cutoff frequencies set to 200 Hz and 3000 Hz, respectively. The spike detector method was "Adaptive Threshold Crossing," with the threshold set to 6x standard deviation. The pre-spike and post-spike durations were set to 0.84ms and 2.16ms with no sample overlap. In the Inter-Spike Interval Threshold settings, the Maximum Inter-Spike Interval was 100ms and the minimum number of spikes set to 5. The mean firing rate estimation window was 10 s and the synchrony parameters window size was 20ms with the spike counter interval set to 1 s. All cell recordings were performed weekly at 37°C in normoxia for 300 s. Spike sorting was performed using Plexon Offline Sorter, v4.3.1. To reduce noise, only wells that registered five or higher spikes under 300 s were further analyzed. For efficient alignment, waveforms were then oriented around the Global Maximum Start and Sort. Sorting was performed semi-automatically using the K-Means Scanner, with the range set from two to four. Waveforms with shapes uncharacteristic of neuronal action potentials were marked as invalid and removed. Noise clusters, identified and isolated by their position in the 2D Cluster View, were also disregarded for increased accuracy. The timeline view was used to remove artifacts caused by movement or electrode malfunction, on the basis of consistent unnatural firing rate. After each well and unit has undergone alignment, sorting and noise/artifact reduction, the average waveform and action potential graph of each unit is recorded. After the last time point recording, 0.1 μM tetrodotoxin was added to block sodium channels and validate that neurons were responsible for the firing detected with the MEA plates (data not shown). At least three independent experiments were recorded for each cell line.

RNA extraction for RNA sequencing

Cortically-differentiated iPSCs were manually scraped off of coverslips at days 0, 60, 80, 100 and 130 in PBS, spun down at 1000 RPM for 5 min and pellets were snap-frozen in liquid nitrogen. Frozen pellets were resuspended in 1 mL Trizol (Thermo Fischer Scientific 155596026). 200 μL of choloroform (Sigma-Aldrich C2432-25ML) was added, then samples were shaken and incubated at room temperature for 3 min prior to spinning at 13,000 RPM for 15 min. The clear supernatant was moved to a new tube and 318 μL of 100% ethanol was added. The supernatant was then transferred to an RNeasy column (QIAGEN 74106) and spun 30 s at 13,000 RPM. Column was washed once with 500 μL buffer RW1 and spun for 30 s at 13,000 RPM. 70 μL of buffer RDD and 10ul of RNase-free DNase (QIAGEN 79254) were added to the column and incubated for 30 min. 500 μL of buffer RW1 was then added and column was spun at 13,000 RPM for 30 s. Column was then washed again with 500 μL of RPE and spun at 13,000 RPM for 30 s. The collection tube was changed and spun at 13,000 RPM for 1 min to remove residual buffer. 50 μL of RNase-free water was added and incubated at room temperature for 3 minutes before being spun into a clean collection tube at 13,000 RPM for 5 min. RNA was quantified using a nanodrop then 500 ng was run on a 1% agarose gel to ensure quality. At least 1,200 ng of RNA was submitted for sequencing.

Library preparation and sequencing

Library construction was performed using the Illumina TruSeq Stranded mRNA library preparation kit (Illumina, San Diego, CA). Briefly, total RNA samples were assessed for concentration using a Qubit fluorometer (ThermoFisher Scientific, Waltham, MA) and quality using the 2100 Bioanalyzer (Agilent Technologies, Santa Clara, CA). Up to one μg of total RNA per sample was used for poly-A mRNA selection. cDNA was synthesized from enriched and fragmented RNA using reverse transcriptase (Invitrogen, Carlsbad, CA) and random primers. The cDNA was further converted into double-stranded DNA (dsDNA), and the resulting dsDNA was enriched with PCR for library preparation. The PCR-amplified library was purified using Agencourt AMPure XP beads (Beckman Coulter, Brea, CA). The concentration of the amplified library was measured with a Qubit fluorometer and an aliquot of the library

was resolved on a Bioanalyzer. Sample libraries are multiplexed and sequenced on a NextSeq 500 platform (Illumina) using 75bp single-end sequencing. On average, about 20 million reads were generated from each sample.

RNA Sequencing

Raw reads obtained from RNA-Seq were aligned to the transcriptome using STAR (version 2.5.0) (Dobin et al., 2013)/ RSEM (version 1.2.25) (Li and Dewey, 2011) with default parameters, using a custom human GRCh38 transcriptome reference downloaded from https://www.gencodegenes.org, containing all protein coding and long non-coding RNA genes based on human GENCODE version 23 annotation. Expression counts for each gene in all samples were normalized by a modified trimmed mean of the M-values normalization method and the unsupervised PC analysis (PCA) was performed with DESeq2 Bioconductor package version 1.10.1 in R version 3.2.2. Each gene was fitted into a negative binomial generalized linear model, and the Wald test was applied to assess the differential expressions between two sample groups by DESeq2. Benjamini and Hochberg procedure was applied to adjust for multiple hypothesis testing, and differential expression gene candidates were selected with a false discovery rate less than 0.05. The HD 180 samples and the CTR21 d130 sample were treated as outliers and excluded, based upon the plot of principle component analysis and hierarchical clustering (at least 3 standard deviations from all other samples; Figure S5). After exclusion of these samples, the N (independent experimental sample) for each ''cell line (time point; 0, 60, 180, 130 days of differentiation)'' is as follows: HD109 (1, 2, 3, 3, 2), HD77 (1, 2, 3, 3, 1), CTR33 (1, 2, 2, 2, 1), CTR21 (1, 2, 3, 3, 0), CTR18 (1, 2, 2, 2, 1). Each replicate sample (per cell line, per time point) was from an independent experimental differentiation. For visualization of coordinated gene expression in samples, a two-way hierarchical clustering with Pearson correlation distance matrix was performed with samples and DEG candidates using the Bioconductor g-plots package (version 2.14.2) in R. The pathway enrichment analysis was performed on these candidates with DAVID (https://david.ncifcrf.gov/summary.jsp) and IPA (QIAGEN). RPKM (reads per kilobase of transcript per million mapped reads) values were calculated for each gene of all samples to compare the gene expression from 524 samples downloaded from ALLEN BRAIN ATLAS database (http://www.brainspan.org/static/download.html). RPKM levels below 1.0 were set to a ''floor'' value of 1.0. Low expression genes were filtered out and expression matrix were subjected to logarithm transformation. Pearson correlation was calculated between 30 samples and 524 samples.

The HD patient BA4 data from (Hodges et al., 2006) was analyzed with GEO2R, Benjamini and Hochberg (FDR) adjustment applied, auto-detect log transformation applied, NCBI generated category of platform annotation to display (GSE3790, GPL96) in order to determine the DEGs between all HD and all control post-mortem samples. All 16 control BA4 regions of the control BA4 cerebral cortex (HD grade 0; Ages 34-81 years) were compared to all 19 HD BA4 regions (HD grade 0-3; Age 41-87).

GO Terms: Gene ontological (GO) analysis was performed using DAVID Bioinformatics database (version 6.8) (Huang et al., 2007b, Huang et al., 2007a). The top or bottom 1000 genes from each PC were uploaded in the functional annotations platform. The background was maintained against *Homo sapiens*. After receiving the summary results through the platform, only 7 categories were selected. ''OMIM_Disease'' under Disease; ''GOTERM_BP_DIRECT,'' ''GOTERM_CC_DIRECT,'' and ''GOTERM_MF_DIRECT'' under Gene Ontology; and ''BIOCARTA,'' ''KEGG_PATHWAY,'' ''REACTOME_PATHWAY'' under Pathways. The functional annotation chart was obtained after the category selection. The resulting chart was rerun using all correction option available. The resulting file was downloaded, opened and sorted in Microsoft Excel to obtain the corrected Bonferroni value of $p < 0.05$. All the terms meeting the criteria were used for further analysis.

WGCNA

WGCNA was performed using its package in R (Langfelder and Horvath, 2008; Zhang and Horvath, 2005), per the instructions found at ''https://horvath.genetics.ucla.edu/html/CoexpressionNetwork/Rpackages/WGCNA/Tutorials/.'' Normalized and log2-transformed data was loaded into R and the samples were clustered, based upon their Euclidean distance. The soft threshold power β of 8 was used, based upon the network topology, as it was the lowest power for scale-free topology fit index curve flattens out upon reaching a high value. The one step network construction and module detection command blockwiseModules was used, with power = 6, maxBlockSize = 23,000, TOMType = ''signed,'' networkType = ''signed,'' minModuleSize = 30, reassignThreshold = 0, mergeCutHeight = 0, numericLabels = TRUE, pamRespectsDendro = FALSE, saveTOMs = TRUE, and verbose = 3. The eigengene expression of the resulting modules, which is the first PC of all expression values of genes assigned to that module, were then correlated to the samples traits (HD and day of differentiation) and P values (corPvalueStudent; calculates Student asymptotic p value for given correlations) were Benjamini-Hochbert corrected for multiple comparisons. The genes for each module found to be significantly correlated to a given trait were then analyzed using DAVID Bioninformatics Database, as described above.

QUANTIFICATION AND STATISTICAL ANALYSIS

Experimental repeat numbers are listed within the methods above for each analysis. Changes in the percent of various immunocytochemical markers and the MEA neuronal firing pattern data were tested across groups and time with mixed model regression to account for the repeated-measures taken within each cell line over time. A compound-symmetry correlation structure was used. Residuals were inspected to confirm the model fit and absence of outliers. Where necessary, data was transformed using Box-Cox method prior to analysis to meet assumptions necessary for parametric assessment. Separate regression models were constructed with similar methods to test the association between HTT CAG repeat number and immunocytochemical counts or neuronal firing.

Post hoc multiple testing performed with the adapted step-down Bonferroni adjustment method at a two-sided alpha level of 0.04. All analysis was performed using SAS v9.4 software. For the single-cell patch clamp experiments, Chi Squared tests were performed on data with a categorical or binomial dependent variable. t tests were performed on data with a continuous dependent variable, following inspection to be sure that the data were normally distributed around each hypothesized mean. Unless stated otherwise, continuous data are reported as mean ± standard error of the mean. All raw data and statistical evaluations can be found in Mendeley (''Human Huntington's Disease iPSC-derived cortical neurons display altered transcriptomics, morphology, and maturation'' https://doi.org/10.17632/y275mydz78.1).

DATA AND SOFTWARE AVAILABILITY

The accession number for the RNA sequencing data reported in this paper is GEO: GSE109534.